

Topical Review

Foundations of physical vapor deposition with plasma assistance

Jon Tomas Gudmundsson^{1,2,*} , André Anders^{3,4} 
and Achim von Keudell⁵ 

¹ Space and Plasma Physics, School of Electrical Engineering and Computer Science, KTH Royal Institute of Technology, SE-100 44 Stockholm, Sweden

² Science Institute, University of Iceland, Dunhaga 3, IS-107 Reykjavik, Iceland

³ Leibniz Institute of Surface Engineering (IOM), Permoserstraße 15, 04318 Leipzig, Germany

⁴ Felix Bloch Institute of Solid State Physics, Leipzig University, Linnéstraße 5, 04103 Leipzig, Germany

⁵ Institute for Experimental Physics II, Ruhr-University Bochum, Germany

E-mail: tumi@hi.is

Received 29 May 2021, revised 16 June 2022

Accepted for publication 7 July 2022

Published 19 September 2022



CrossMark

Abstract

Physical vapor deposition (PVD) refers to the removal of atoms from a solid or a liquid by physical means, followed by deposition of those atoms on a nearby surface to form a thin film or coating. Various approaches and techniques are applied to release the atoms including thermal evaporation, electron beam evaporation, ion-driven sputtering, laser ablation, and cathodic arc-based emission. Some of the approaches are based on a plasma discharge, while in other cases the atoms composing the vapor are ionized either due to the release of the film-forming species or they are ionized intentionally afterward. Here, a brief overview of the various PVD techniques is given, while the emphasis is on sputtering, which is dominated by magnetron sputtering, the most widely used technique for deposition of both metallic and compound thin films. The advantages and drawbacks of the various techniques are discussed and compared.

Keywords: physical vapor deposition, magnetron sputtering, cathodic arc deposition, ion beam deposition, sputtering, pulsed laser deposition

(Some figures may appear in colour only in the online journal)

1. Introduction

The formation of a condensable vapor by physical mechanisms and subsequent deposition of this material onto a substrate as a thin film or coating is referred to as physical vapor deposition (PVD) (Mahan 2000, Rossnagel 2003, Thornton 1988). The formation of a vapor refers to a phase transition of the film-forming material from a solid or liquid phase into a gaseous or

plasma phase. PVD is a broad field and various processes are applied to create film-forming material and to achieve thin film deposition. Physical vapor can be created by a wide range of techniques, which have in common that the atoms are removed from a solid or liquid source by physical means, momentum exchange via thermal evaporation, sublimation, ion sputtering, electron beam and laser ablation, and/or arc-based emission. Historically, vapor was descriptive for the film-forming material in evaporation processes, as atoms in a vapor can be characterized by the equilibrium parameter temperature. However, when describing most modern PVD techniques, the term ‘vapor’ (the gas phase of a substance at a temperature lower than its critical temperature) is somewhat of a misnomer

* Author to whom any correspondence should be addressed.



Original content from this work may be used under the terms of the [Creative Commons Attribution 4.0 licence](https://creativecommons.org/licenses/by/4.0/). Any further distribution of this work must maintain attribution to the author(s) and the title of the work, journal citation and DOI.

since we do not simply deal with the gas phase but with a non-isotropic, directional flux of particles. All forms of sputtering, pulsed laser deposition (PLD), and arc processes deliver fluxes characterized by a preferred direction and the presence of energetic particles. Often the film-forming material is composed of atoms or small clusters of atoms of elements that cannot easily be prepared as a gas phase plasma precursor. The chemical reactions in the PVD process occur almost entirely on a surface, preferably the substrate surface.

PVD processes are often categorized into equilibrium and non-equilibrium processes depending on the ways in which the source material is vaporized. The equilibrium processes include thermal evaporation, by conventional resistive heating, as well as electron-beam evaporation. Deposition methods that are based on thermal evaporation include molecular beam epitaxy (MBE) and ion plating. Evaporation is easiest to achieve by simply heating the source material, that is placed in an evaporation crucible, with a hot filament or conventional resistive heating. These methods are often combined with a plasma discharge, that either provides radicals to the process or ionizes the evaporated atoms. In the latter case, a discharge is created, located between the evaporant and the substrate, and the evaporated atoms are ionized as they travel through the discharge. In other cases, the evaporation deposition is accompanied by simultaneous ion bombardment of the growing film by ions from an ion source. In non-equilibrium evaporation, the film-forming material is fed from an open source, often liquid material that evaporates off into a large, low pressure volume. Non-equilibrium processes include sputtering, by ions from a plasma discharge or by ion beams accelerated from a dedicated ion source.

Plasma-based PVD processes often use a plasma discharge as the source of ions for a sputter process, or the sputter process is driven by ions from an ion source. In both cases the ions are accelerated to a solid target, which is the source of the material to be deposited, the film-forming material. The positive ions are preferentially ions of a heavy inert gas such as argon. In the former case, sputter deposition is driven by positive ions from a plasma discharge that is created and maintained through electron impact ionization of a low pressure inert working gas. As the ions bombard a negatively biased target (the cathode) composing the source material, atoms of the film-forming material are ejected and fall onto and coat a substrate. The film-forming species released from a solid or liquid by evaporation or sputtering are generally neutral atoms. Often the sputtered species are made to travel through a discharge where they are ionized, either intentionally or unintentionally. Furthermore, the ion bombardment, in the case of sputtering, also induces emission of secondary electrons. In fact the discharges are maintained by secondary electron emission from the cathode (diode sputter source) or by Ohmic heating, or the combination of the two (magnetron sputtering discharge). Another plasma-based PVD process is cathodic arc (including vacuum arc) deposition, characterized by a high flux of ionized cathode material.

The energy, or more precisely the energy distribution, of the film-forming species can have a significant influence on the properties of the deposited film. Whereas thermal

evaporation provides film-forming species at typical thermal energies, significantly below 1 eV, sputter techniques provide energetic neutrals of a few eV, as these originate from a collision cascade in the solid when an ion impinges onto a target material to be transferred to the substrate. PLD and arc deposition create species with even higher energies, which can in both cases exceed 100 eV. Thereby, the various PVD techniques provide film-forming species that can span a wide range in energy. Figure 1(a) shows the typical range of particle energy in the substrate vicinity for a few PVD techniques. The particle energy varies over a wide range both within each technique and between the different techniques. Figure 1(b) shows the growth rate range for the different PVD techniques. The resulting film growth rates also vary over a wide range between the different PVD processes. Thermal evaporation deposition has the highest growth rate but exhibits the lowest energy of the film-forming species, while the growth rate of ion beam and PLD is low, but the energy of the film-forming species is high. Also, the ionization fraction of the film-forming species varies between the different methods. In thermal evaporation the film-forming species are mostly neutral, while arc deposition and PLD produces highly ionized flux of the film-forming species. These process parameters, deposition rate, energy of the film-forming species and their ionization fraction dictate the microstructure of the deposited film, and therefore the properties of the resulting films or coatings. The influence of the ionization fraction in the deposition flux on the film surface morphology is demonstrated in figure 2, which was obtained by molecular dynamics simulations of copper film growth, comparing fully neutral deposition flux (thermal evaporation), 50% ionization and 100% ionization (PLD, cathodic arc) of the deposition flux (Kateb *et al* 2019). Thermal evaporation deposition gives films that exhibit very rough surfaces as seen in figure 2(a), while with increased ionization of the deposition flux the films exhibit increasingly smoother surface as seen in figure 2(b) for 50% ionization, and for fully ionized deposition flux in figure 2(c). It is clear from this comparison that the ionization fraction has a significant influence on the microstructure and surface morphology of the resulting film.

Apart from the growth rate, the energy of the film-forming species and the ionization fraction, there are a number of other issues that have to be considered when choosing a deposition method for a given application. By application of magnetron sputtering, the film properties such as the crystalline phase, microstructure, stress, morphology, mechanical properties, optical properties, and electrical resistivity can be tuned by adjusting the applied power and working gas pressure, while in thermal evaporation deposition there is no control over the energetics of the evaporated species and the resulting film properties. In sputter deposition, the composition of alloy targets is generally reproduced in the deposited film, while in thermal evaporation the composition of the resulting film depends on the relative vapor pressure of the constituent elements, which makes it a challenge to deposit alloys. In recent decades there has been a trend of combining the different deposition techniques for thin film deposition, surface modification, or surface treatment, in order to optimize throughput, and to achieve the desired thin film properties.

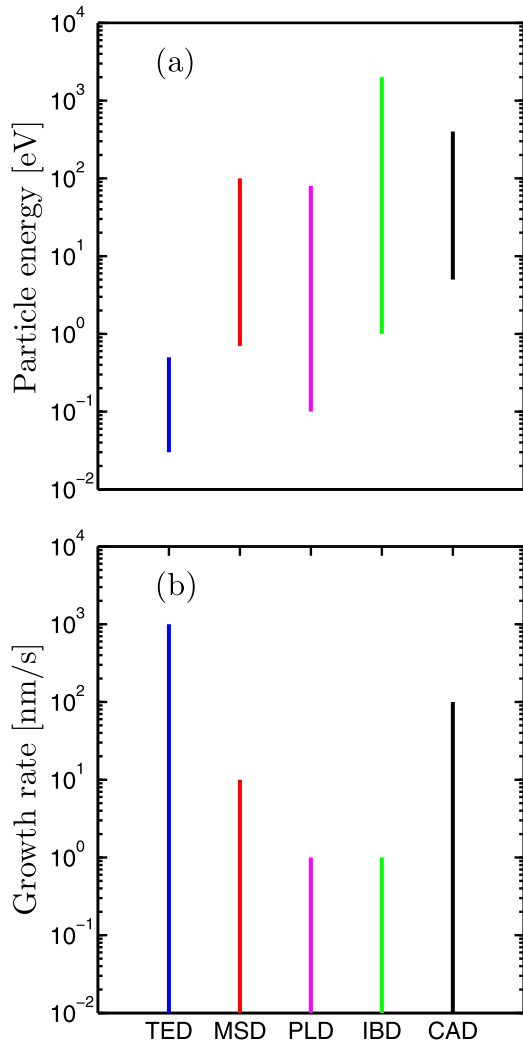


Figure 1. The typical (a) range of particle energy at the substrate and (b) growth rate for the various PVD methods: thermal evaporation deposition (TED), magnetron sputtering deposition (MSD), pulsed laser deposition (PLD), ion beam deposition (IBD) and cathodic arc deposition (CAD). Based partially on Bundesmann and Neumann (2018), while for the cathodic arc the deposition rate is based on Goldberg *et al* (2012) and the energy range is based on Anders and Yushkov (2002) and Byon and Anders (2003).

Both the substrate temperature (or the film temperature) and the energy of the film-forming species influence the microstructure of deposited polycrystalline films. This can be shown by a structure zone diagram that incorporates both the deposition temperature and the energetic deposition, which is typically due to a large flux of ions (Anders 2010). Such a structure zone diagram where the variables are a generalized temperature T^* , a normalized energy flux E^* , and the net film thickness t^* , is shown in figure 3. The generalized temperature T^* , which includes both the film temperature, and the potential energy of the particles that arrive on the substrate, is defined as

$$T^* = T_h + \frac{1}{k} \frac{\sum_{\alpha} (\mathcal{E}_{\text{pot}} J_{\alpha} / N_{\text{moved},\alpha})}{\sum_{\alpha} J_{\alpha}}, \quad (1)$$

where $T_h = T/T_m$ is the film temperature normalized by the melting temperature T_m of the deposited film, J_{α} is the ion current density onto the substrate, $N_{\text{moved},\alpha}$ is the number of atoms that are rearranged on the surface, and the potential energy is

$$\mathcal{E}_{\text{pot}} = \mathcal{E}_{\text{ce}} + (\mathcal{E}_{\text{iz}} - \phi), \quad (2)$$

and \mathcal{E}_{ce} is the heat of sublimation, or the cohesive energy, \mathcal{E}_{iz} the ionization energy, and ϕ the work function of the electron for neutralization. The generalized kinetic energy is given as

$$E^* = \frac{\sum_{\alpha} ((\mathcal{E}_{\text{kin},\alpha} M_{\alpha}) / (\mathcal{E}_{\text{ce}} M_s)) J_{\alpha}}{\sum_{\alpha} J_{\alpha}} \quad (3)$$

where M_{α} is the mass of the energetic particle, M_s is the mass of an atom in the deposited film. The structure zone diagram (figure 3) shows that the film morphology varies from tapered crystallites separated by voids (zone 1) to an array of fibrous grains separated by grain boundaries (zone T) to columnar grains extending to the entire coating thickness (zone 2), and to large grains with flat tops (zone 3), with increased film temperature. Higher film temperatures lead to increased diffusivity of the film atoms during growth and therefore increased grain size.

The dependence of the film properties on the parameters E^* and T^* , as shown in figure 3, illustrates that the temperature T^* can be partly replaced by the energy of the incident ions E^* , because similar film structures (as characterized by the different deposition zones in figure 3) are obtained at lower temperature T^* but higher E^* . Therefore, as the generalized energy E^* is increased the transition temperature between the neighboring zones is shifted to lower values of both t^* and T^* . On the microscopic level, this is explained by the higher adatom mobility of energetic species contributing to film growth at higher E^* . The term adatom is short for adsorbed atom and the diffusion of this atom along the surface is referred to as adatom mobility. Adatom mobility can be influenced not only by thermal energy but also by energetic particle bombardment. From a technological perspective, this has significant advantages. A typical application scenario of PVD process is the deposition of hard ceramic coatings on metal work pieces. In a purely thermal evaporation deposition process, such hardness could only be reached at very high substrate temperatures, where the hardened metal substrate unfortunately becomes weakened again. This is avoided in ion-driven deposition processes, where the metal substrates can remain at much lower deposition temperature during the application of the PVD coating, due to bombardment of energetic species.

Here, we review the various PVD techniques that have been developed for thin film deposition, while the main emphasis is on ion-driven plasma discharge-based approaches, including diode and magnetron sputtering, as well as cathodic arc, and PLD. In the following, we start with the discussion of simple thermal and electron beam evaporation processes in section 2, which are often initiated by a plasma or are being combined with a plasma discharge. This is followed by discussion of the various plasma-based PVD methods in section 3, where the main emphasis is on the magnetron sputtering discharge and

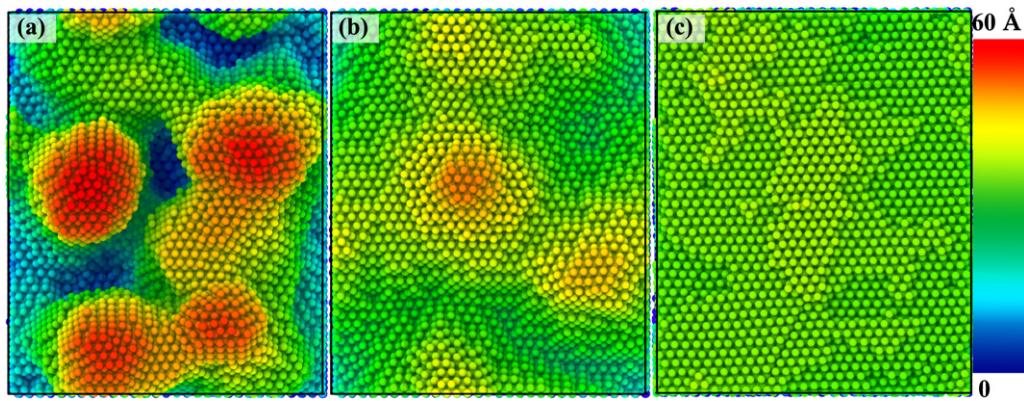


Figure 2. Surface topology of copper films obtained by molecular dynamics simulations assuming (a) fully neutral deposition flux, (b) 50% ionization of the deposition flux, and (c) full ionization of the deposition flux, while assuming the same deposition time and energy distribution of the film-forming species. The deep blue indicates substrate surface and red denotes thickness higher than 6 nm. Reprinted with permission from Kateb *et al* (2019). Copyright 2019, American Vacuum Society.

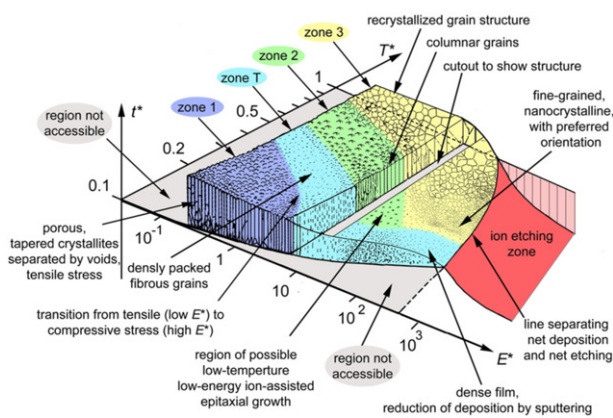


Figure 3. A structure zone diagram based on a generalized temperature T^* , a normalized energy flux E^* , and net film thickness t^* . Reprinted from Anders (2010), Copyright (2010), with permission from Elsevier.

its variations, and finally we discuss cathodic arc deposition in section 4.

2. Evaporation

To deposit thin films by evaporation, in a vacuum environment, sufficient amount of heat has to be provided to the evaporant. The evaporation can be driven by thermal heating (resistance or induction heating), electron beam heating or laser ablation of a source material. Note that thermal evaporation in high vacuum is not a plasma supported deposition process as the film-forming species are neutral atoms. Evaporation methods based on heating where the evaporation process is nearly in steady state equilibrium with its vapor (effusion or Knudsen cell) are the basis for deposition techniques such as MBE, where the vapor is composed of neutral atoms.

2.1. Thermal evaporation

The first commercial thin film deposition technique was thermal evaporation or resistance heated evaporation, where the evaporants are placed in a boat or a crucible. Typically, the boat is made of a refractory metal, such as tantalum or tungsten, which is heated by passing a large current through the band of metal forming the boat. A crucible is typically a ceramic cup that is wrapped with a metal wire coil which is resistively heated by passing a current. The evaporation rate is generally proportional to the evaporation temperature and consequently dependent on the power density delivered to the source. The energy distribution of the evaporant is determined by the thermodynamics at the evaporation temperature. For evaporation occurring around 800–1300 K, which is common temperature range used, the kinetic energy of the evaporated species is small (see figure 1(a)) compared to the chemical bond strength of a solid film and therefore, it has little effect on the deposition mechanism, the film growth, and film quality. The typical energy range of the evaporated atoms is 0.03–0.5 eV. Thermal evaporation is typically performed at sufficiently low background pressure ($\sim 10^{-4}$ Pa) so that the evaporated atoms are transported to the substrate without collision and therefore thermal evaporation is a ‘line-of-sight’ process. The evaporated material then condenses on a substrate which is kept at a suitable temperature. The resulting film microstructure is columnar, separated by voids, which is denoted as zone 1 and maybe zone T in the structure zone diagram of figure 3. This occurs because of limited surface mobility of the evaporated atoms on the substrate, during growth. Furthermore, the surface morphology is rough as can be seen in figure 2(a).

When both solid and/or liquid states and vapor states exist simultaneously at a common temperature in an enclosed chamber the equilibrium pressure is referred to as vapor pressure or saturation vapor pressure. Then, equal number of atoms of the solid and/or liquid enters the gaseous phase in comparison to the atoms that condense, the evaporation rate is equal to the

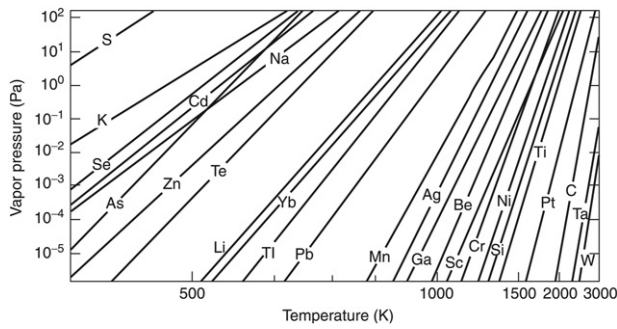


Figure 4. The vapor pressure versus temperature for various elemental materials. Reprinted from Gall (2005), Copyright (2005), with permission from Elsevier.

condensation rate. The vapor pressure is temperature dependent. The vapor pressure that develops over a solid or liquid can be estimated using the Clausius–Clapeyron equation

$$\frac{dp_v}{dT} = \frac{\Delta H_v}{T(v_g - v_s)} \quad (4)$$

where H_v is the heat of vaporation, v_g the molar volume of the vapor, v_s the molar volume of the sublimating solid and/or the evaporating liquid. The molar volume in the liquid or solid state is very small in comparison with that of the vapor phase so that $v_g - v_s \approx v_g \approx RT/p_v$, where R is the universal gas constant, and

$$\frac{d(\ln p_v)}{d(1/T)} = -\frac{\Delta H_v}{R}. \quad (5)$$

If the heat of evaporation is assumed to be a constant we find

$$p_v \propto \exp(-\Delta H_v/RT). \quad (6)$$

The exponential dependence of the vapor pressure with temperature indicates that small variations in temperature can lead to large changes in the vapor pressure and the condensation rate. The vapor pressure is shown versus temperature for various elemental materials in figure 4.

The main advantages of thermal evaporation deposition are high-deposition rates and that the source material can be supplied in a simple form. The rate of evaporation is given by the Hertz–Knudsen equation

$$\frac{1}{A} \frac{dN}{dt} = \frac{\alpha_v}{\sqrt{2\pi M k_B T}} (p_v - p), \quad (7)$$

where A is the emitting surface area, N is the number of gas atoms or molecules, α_v the evaporation coefficient, p_v is the equilibrium vapor pressure at the evaporant surface, p is the hydrostatic pressure acting on the surface, M is the molecular weight of the evaporated atoms, k_B is Boltzmann's constant and T is the temperature. The flux of material evaporating from a circular area of uniform temperature exhibits a cosine angular distribution, with its maximum normal to the emitting area. The arrival rate onto a substrate can be calculated assuming a cosine angular distribution to account for the relative positions and orientations of the substrate and emitting areas. This gives an arrival rate or the number of particles incident upon a

unit surface area per unit time called the impingement rate Φ (molecules $\text{cm}^{-2} \text{s}^{-1}$) (Harper 1990)

$$\Phi = \frac{\alpha_v A \cos \phi \cos \theta}{\pi r^2 \sqrt{2\pi M k_B T}} (p_v - p), \quad (8)$$

where ϕ is the angle from source normal to substrate, θ is the angle from substrate normal to the source, and r is the source-to-substrate distance. This leads to a deposition rate DR on the substrate

$$\text{DR} = 10^7 \frac{M \Phi}{\rho N_0} \text{ (nm s}^{-1}\text{)}, \quad (9)$$

where ρ (g cm^{-3}) is the deposited film mass density, M (g/mole) is the molecular weight of the evaporating species, and N_0 is Avogadro number. However, due to the roughly exponential dependence of vapor pressure on temperature (equation (6)) it is a challenge to control the flux from the source. Under typical vacuum deposition conditions, the vaporizing material is not in equilibrium with its vapor, however it arrives at the substrate at the impingement rate given by equation (8) at the given vapor pressure determined by the source temperature. Due to this thermal evaporation deposition systems have to be feedback controlled based on measuring the deposition rate.

Evaporation is very effective for depositing materials of high vapor pressure (which are often materials of low melting point). A major drawback of thermal evaporation deposition is the difficulty in forming alloy films from a single crucible (Rossnagel 2003). As each element has its own temperature–vapor pressure relation the evaporation rate of two elements in a common crucible or boat is generally very different. The element with higher vapor pressure will evaporate at a higher rate, leaving behind the lower vapor pressure element. The substrate will therefore receive first the higher vapor pressure element and at a lower rate the lower vapor pressure element. This can be solved by having a source crucible for each element and adjust the flux to the desired level. This is referred to as co-evaporation, but it is a challenge to operate in controlled manner. Therefore, due to these difficulties thermal evaporation is typically not used to deposit alloy films.

The film microstructure can be greatly improved, resulting in enhanced film properties, if the depositing film is bombarded with energetic particles (ions and/or neutrals). One approach to improve the properties of evaporated thin films is ion plating, which is discussed in section 2.3. Another approach is called metal-vapor plasma deposition. Then, the evaporated flux is directed through an electrodeless discharge as it travels toward the substrate. This has been demonstrated using electron cyclotron resonance (ECR) discharge to ionize the copper vapor that was thermally evaporated (Holber 2000, Holber *et al* 1993). This setup is shown in figure 5. A microwave (2.45 GHz) is fed into a vacuum chamber through a quartz window. Four electromagnets create the magnetic field required for efficient microwave absorption, creation of a discharge, and transport of the plasma to the substrate. Copper is evaporated from a resistively heated source, which is continuously replenished through the use of an in-vacuum wire feeder. The evaporated copper atoms enter the resonance zone of the discharge, the plasma is created from the evaporated metal, and

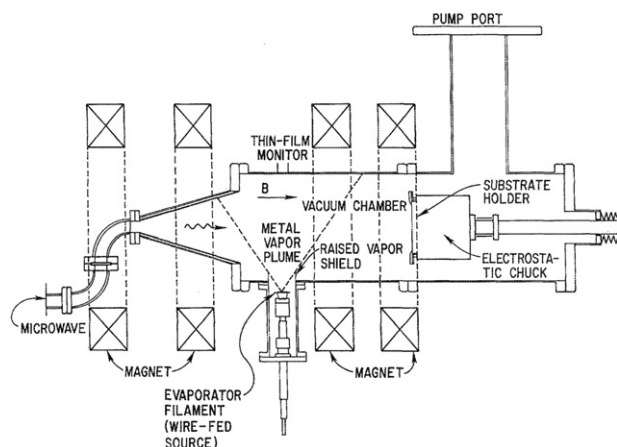


Figure 5. ECR discharge based ionization of evaporated copper apparatus. The copper atoms are introduced into the vacuum chamber from a thermal evaporator located underneath the chamber. Reprinted with permission from Holber *et al* (1993). Copyright 1993, American Vacuum Society.

no working gas is needed during the deposition. This approach has been demonstrated to give copper flux at the substrate that is nearly 100% ionized (Holber *et al* 1993). The substrate itself is not placed line-of-sight of the thermally evaporated copper.

2.2. Electron beam evaporation

The electron beam evaporation sources differ from thermal evaporation sources in two fundamental ways: the heating energy is supplied onto the top of the evaporant as the kinetic energy of a high current electron beam. The incident e-beam only melts a relatively small area on top of the source material. This small area is heated well above the melting point, while the temperature of most of the source material is much lower, as the hearth is typically water-cooled. Therefore, the molten source material is only in contact with a de-facto crucible made of the same material, and any chemical reactions with contaminants, such as the crucible, are eliminated. The use of an electron beam therefore eliminates the limitations caused by the need to reach the melting point of materials that can be evaporated.

The electron beam evaporation source is composed of three basic components: the electron gun, the beam deflection magnetic lens, and the evaporant containing hearth. The electron beam typically originates from a filament located from underneath the hearth, passes through the magnetic lens and is focused upon the evaporant, so the filament is not in line-of-sight of the point of evaporation. This approach has the benefit that a very high power density can be provided, and hence a wide range of control over evaporation rates from very low to very high, can be achieved. These components and the crucible are typically constructed as an integrated assembly as shown in figure 6. Typically the electron beam is accelerated to about 10 keV and the electron current can be as high as 1.5 A. This beam impacts an area of up to 1 cm² with a power density of up to 60 kW cm⁻² (Graper 2017).

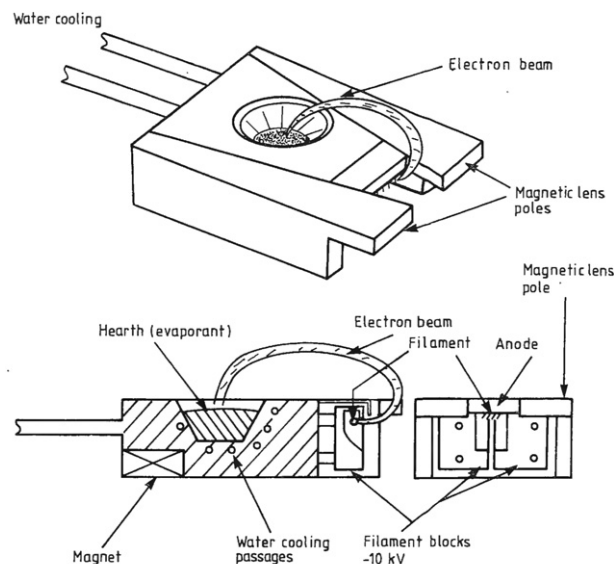


Figure 6. A schematic of an electron beam heated evaporation source. The electron beam originates from a filament located from underneath the hearth, passes through the magnetic lens and is focused upon the evaporant. Graper (2017), reprinted by permission of the publisher (Taylor & Francis Ltd, <http://tandfonline.com>.)

2.3. Ion plating

Ion plating refers to an evaporation deposition process in which the substrate or the growing film experiences in addition to the flux of evaporated species a continuous or periodic flux of energetic species that influences the deposition process and consequently the resulting film properties (Mattox 1998, chapter 8). When positively charged ions are accelerated toward a negatively biased substrate, in an otherwise thermal or electron beam evaporation process, it is coined ion plating (Martin 1990). These can be either ions of the evaporated film-forming species or more often the ions of an inert working gas. Ion plating was initially applied to improve film adhesion and the surface coverage of the deposited films, but soon came the understanding that bombardment by energetic particles could enhance film properties, such as film mass density and residual film stress. Ion plating also provided the possibility to sputter clean the substrate with argon ions before depositing a film. For a more thorough discussion on ion plating the reader is referred to the reviews by Mattox (1998, chapter 8) and Stelmack *et al* (1989).

The ion plating system can be either 'plasma-based' or 'vacuum-based'. Evaporation can be driven by either resistive or electron beam heating of the evaporant. Plasma-based ion plating can include evaporation that is carried out in a plasma environment where a fraction of the evaporated atoms are ionized in a plasma discharge. Ionization can also be achieved by having the electrons or an electron beam that drives the evaporation also pass through the vapor of the evaporant. These ions can then be accelerated toward the substrate by an electric field applied using an external voltage supply to create a potential between the evaporation source

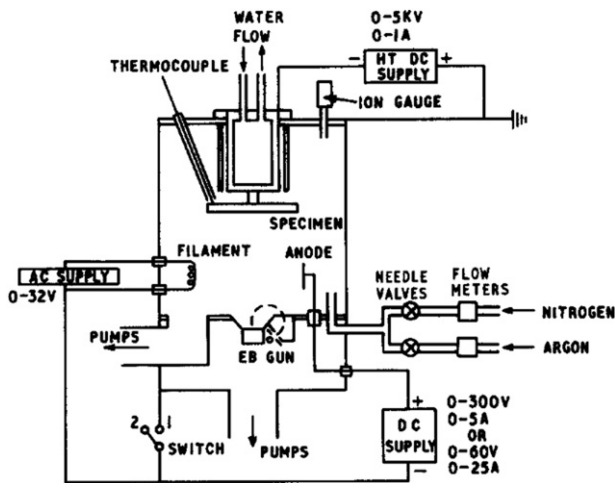


Figure 7. A schematic of plasma-based ion plating or a thermionically assisted triode coating system. The source of the film-forming material is electron beam evaporation. The substrate acts as a cathode with bias voltage of up to 5 kV. Reprinted from Matthews and Teer (1980), Copyright (1980), with permission from Elsevier.

and the substrate. One approach is to generate a dc glow discharge by applying a highly negative voltage to the substrate. The working gas is often argon that is maintained at pressure of 1–10 Pa and negative voltage of 3–5 kV is applied to the substrate. The substrate is therefore submersed in a plasma and is negatively biased, and therefore can act as a cathode. The sheath that forms is collisional and the positive ions and neutrals that bombard the substrate exhibit a broad energy spectrum. The energy distributions of both ions and neutrals range from zero to the energy corresponding to the cathode potential. Teer (1976) estimates that for every energetic ion arriving at the cathode at least 14 energetic neutrals arrive and that the average energy of an arriving ion is about 1/10 of the cathode potential while the average energy of the neutrals is 1/22 of the cathode potential. The plasma can also be generated by electron beam (thermionic triode), by a hollow cathode source (Morley and Smith 1972) or an inductively coupled discharge (Murayama 1974). The substrate can be positioned either in the active plasma region or at a remote or downstream position. This approach is sometimes referred to as ion assisted deposition or ion vapor deposition.

A schematic of a plasma-based ion plating system with an electron beam evaporation source delivering the film-forming material is shown in figure 7. The system employs a positive electrode which has the purpose of extracting electrons generated in the vapor source region to increase ionization. A hot filament electron source is incorporated and serves the role of improving controllability, to increase ionization, and to permit a smooth transition from the etch to the deposition mode.

In ‘vacuum-based’ ion plating, the substrate is deposited in vacuum and the ion bombardment is achieved by a separate ion source. In that case the source of vaporization can be sep-

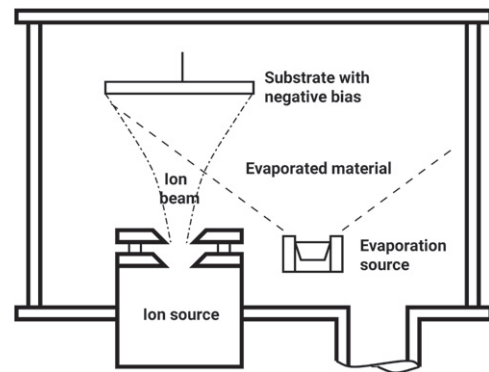


Figure 8. A schematic of IBAD system. It consists of evaporation source for the film-forming material and an ion source that directs ions onto the substrate. Based on Aisenberg and Chabot (1973).

arate from the source of energetic ions, while the evaporation flux and ion bombardment are simultaneous. This is referred to as ion beam assisted deposition (IBAD) and was originally introduced by Aisenberg and Chabot (1973). A schematic of an IBAD system is shown in figure 8. The ion sources used for IBAD are typically of a broad-beam design (Kaufman source) (Kaufman and Robinson 1989), while other ion sources are also used. The IBAD technique has been reviewed by Rauschenbach (2002).

2.4. Pulsed laser deposition

PLD or laser ablation utilizes a high-energy pulsed laser beam as an excitation source and the photon energy is coupled to a solid bulk target material via electronic processes. As the energetic photon beam is directed onto a solid target it can induce laser ablation and evaporation of the target material. The nature of the interaction of a photon beam with a solid target depends on the power density, pulse duration, wavelength, as well as the optical and thermodynamical properties of the solid material.

The setup of a PLD system is shown schematically in figure 9. The laser beam is introduced into a vacuum chamber, through an optical window, where it is focused onto the target surface. Upon laser ablation, the target material vaporizes and the constituents are transported onto a substrate to be deposited as a thin film. A typical target-to-substrate distance is 2–10 cm. The chamber background pressure is maintained well below 10^{-6} Pa using a vacuum pumping system. Often the chambers hold target manipulators for multiple targets, which makes it possible to fabricate multilayered structures using different target materials. An example of the construction of a PLD system is given by Ye *et al* (2021). Various gases such as oxygen, nitrogen, argon, and hydrogen can be introduced through the gas inlet during thin film deposition to promote gas-phase reactions of the ablated species. Reactive background gas is then introduced into the process chamber to incorporate e.g. oxygen or nitrogen into the growing films. Furthermore, a background gas is also sometimes used to act as moderator of the kinetic energy of the arriving species.

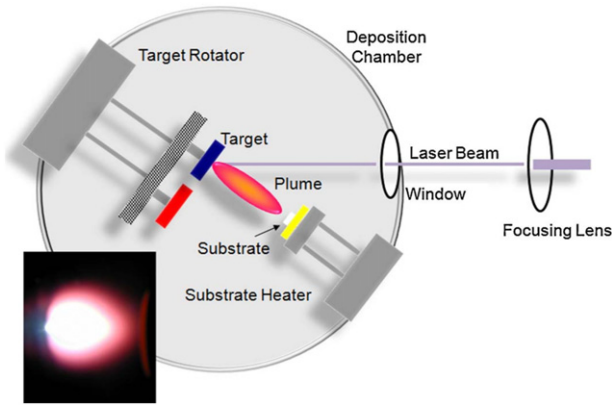


Figure 9. A schematic of a typical PLD setup. A laser beam is introduced through an optical window and focused onto a target surface. Upon laser ablation, the target material vaporizes and the constituents are transported onto a substrate where they form a thin film. The inset picture shows an actual photograph of the plume. Reprinted from Martin *et al* (2010), Copyright (2010), with permission from Elsevier.

When the laser power density reaches a certain value, material is removed from the solid target in the form of a luminous plume. Then the absorption of the incident laser beam energy by the target surface leads to ablation. The threshold power density needed for ejecting a plume depends on the target material, its morphology, and the laser pulse wavelength and duration. The electric field amplitude of an electromagnetic wave is given by (Willmott and Huber 2000)

$$E = \left(\frac{2p_p}{cn\epsilon_0} \right)^{1/2} \quad (10)$$

where p_p is the power density, c is the velocity of light, ϵ_0 is the permittivity of free space, and n is the refractive index of the solid target. For a radiation with power density 500 MW cm^{-2} the electric field strength is of the order of $\sim 10^7 \text{ V m}^{-1}$, which is sufficient to cause dielectric breakdown in many materials. Note that the power density is proportional to the laser fluence and inversely proportional to the laser pulse duration τ_p . Typical values for the applied laser power densities are $50\text{--}500 \text{ MW cm}^{-2}$ for ablation using ultraviolet (UV) excimer laser pulses of 10 nanosecond duration. In principle, any photon beam or laser with sufficient output power can be applied to induce evaporation.

The temporal evolution of the photon beam ablation processes is summarized in figure 10 for a nanosecond long pulse. The processes include laser photon energy absorption at the surface and material excitation, temperature rise followed by surface melting, ablation and plasma formation, laser–plasma interaction, shock wave formation, and plume collapse. The ablation processes can be broadly classified into three regimes separated by different time zones (shown in dotted lines in figure 10). There are differences between nanosecond and femtosecond laser ablation processes, as in the femtosecond case, the plasma is formed after the pulse end, while for the nanosecond pulse the plasma is formed during the pulse and portion

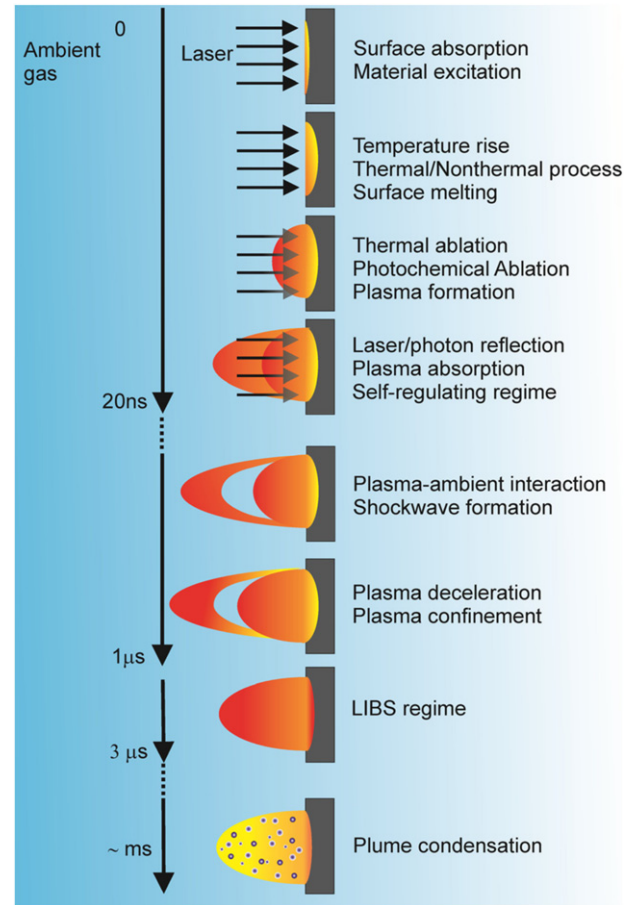


Figure 10. Approximate time scales of laser energy absorption and ablation process using nanosecond laser pulses, along with the various processes that accompany it. Reprinted from Hussein *et al* (2013), with the permission of AIP Publishing.

of the pulse energy reheats the plasma. As the pulse width is reduced to sub-picosecond, i.e. shorter than the time scale of the electron–phonon coupling (a few picoseconds), the ablation process becomes a direct solid–vapor (or solid–plasma) transition.

The first stage of the laser ablation process (i) is the photon absorption by the target surface, as the photon energy of the incident laser beam is converted into electronic excitations which is subsequently transformed into thermal, chemical, and mechanical energy. The photon beam irradiation is absorbed within the surface region of the solid target and the electromagnetic energy is immediately converted into electronic excitation as plasmons, unbound electrons and, in the case of insulators, excitons. The penetration depth depends on the absorption coefficient for the solid target α_s at the given laser wavelength as dictated by the Beer–Lambert law, so that small absorption coefficients result in larger penetration depths. Consequently, the temperature in the vicinity of the irradiated area rises up to several thousands Kelvin. Often the material removal depends on the rate of thermal conduction through the lattice. If the thermal diffusion length, given by $l_T = 2\sqrt{D\tau_p}$, where D is the thermal diffusion coefficient, is smaller than $1/\alpha_s$, the bulk

will be heated down to $1/\alpha_s$, independent of pulse duration. Furthermore, shorter wavelengths also lead to shallower light penetration depths and consequently lower threshold fluences and ablation rates. Transfer of energy from the electrons to the lattice occurs within a few picoseconds, and heating of the absorption layer will begin. When the laser pulse duration is shorter than the electron–phonon coupling process, conventional thermal absorption is significantly limited, and other thermophysical effects play more important roles. For pulse lengths τ_p that exceed the electron–phonon coupling time, the electron–phonon coupling leads to material ablation that proceeds via conventional heat absorption. This process is limited within a depth of tens to hundreds of nanometers. However, the thermal diffusion lengths are only of this order when using femtosecond pulses. Therefore, only when $1/\alpha_s \ll \ell_T$ the photon energy is efficiently thermally transported and deposited into the absorption layer. For metals, the optical absorption depth is smaller than the thermal diffusion length. Therefore, the energy from the laser pulse is first transferred into the absorption layer, followed by a thermal transport of the order of the thermal diffusion length, which is proportional to $\sqrt{\tau_p}$. For ceramics, the thermal diffusion length is shorter than the optical absorption depth and the target will be heated over a distance similar to the optical absorption depth, regardless of pulse duration. This makes it possible to achieve significant material removal even at low laser fluence and with minimum ionization.

During the second stage (ii), the photon absorption is followed by target material vaporization and formation of plasma. Species in the heated area are ejected from the target creating a plume while they continue to absorb energy from the photon beam. This is particularly the case for excimer lasers that exhibit pulses lasting several tens of nanoseconds. For pulses shorter than 1 picosecond, the plasma forms at the end of a laser pulse. The laser ablation creates a plume that is composed of a mix of various species, including electrons, positive and negative ions as well as neutrals, all of which can be in either excited or ground states. Furthermore, there can be diatomics and clusters in the plume. The main absorption process in the plume is inverse bremsstrahlung, which involves the attenuation of the photon flux by inelastic scattering with free electrons. The heating of the plasma plume is determined by the plasma absorption coefficient α_p , which depends on the plasma temperature, wavelength, pulse duration and the species density in the plasma plume, which in turn depends on the degree of ionization, evaporation rate, and the plasma expansion velocities. The absorption coefficient for the plasma plume can be expressed as (Ready 1971, Spitzer 1956)

$$\alpha_p = \left(\frac{4}{3}\right) \left(\frac{2\pi}{3k_B T}\right)^{1/2} \left(\frac{n_e n_i Z^2 e^6}{h c m_e^{3/2} \nu^3}\right) [1 - \exp(-h\nu/k_B T)], \quad (11)$$

where Z is the average charge, n_e is the electron density, n_i is the ion density, T is the plasma temperature, h Planck's constant, and ν is the frequency of the laser light (e.g., infrared

radiation is stronger attenuated than UV radiation). Note in particular that the absorption coefficient scales as $\propto n_e n_i$ and therefore the plasma plume absorbs the incident laser radiation mainly at distances very close to the target surface where the densities of the charged particles are very high. The ablation rate exhibits a strongly decreasing process efficiency as the fluence increases and this has been related to light attenuation and extinction in the laser-induced plasma/vapor plume. For lasers in the infrared, inverse bremsstrahlung is known to be the dominating absorption mechanism, while the effect of inverse bremsstrahlung is expected to play a minor role for excimer laser ablation. Also the wavelength does not only affect the absorption by the target material but also the absorption by the resulting plasma plume, which has higher absorption at longer wavelengths. The plume ionization toward the end of the laser pulse is in the range 10%–100%, but then decreases again due to electron recombination as the plume travels toward the substrate.

The third stage (iii) is the expansion of the plume as the ejected species (which may include atoms, molecules, electrons, ions, clusters, and micron-sized particulates) travel away from the target surface at high mass transport velocity as the ablated species travel toward the substrate. In most cases, PLD is a strongly forward oriented deposition technique and most of the deposited material is contained within an angular range of $\pm 30^\circ$ (Ojeda-G-P *et al* 2018). Finally, the material that composes the plume condenses on a substrate as a thin film.

Typically, PLD uses nanosecond pulses, since for longer pulses thermal effects with droplet formation can dominate. For ultrashort (femtosecond) pulse nanoparticles are often produced, which may be desired for some specific applications. The common pulsed laser sources include a CO₂ laser ($\lambda = 10.6 \mu\text{m}$), Nd–YAG laser (1064 nm) and up to the fifth harmonic outputs (213 nm), femtosecond lasers using hybrid dye/excimer and Ti:sapphire as well as XeCl (308 nm), KrF (248 nm), ArF (193 nm), and F₂ (157 nm) excimer lasers.

The advantages of photon beam evaporation include (i) the production of ionized and excited species with high kinetic energies, (ii) numerous compounds can be evaporated in a similar way with negligible heating of the target, (iii) instantaneous control of the evaporation process, and (iv) high vacuum compatibility. The PLD technique is limited by the fact that the area of the photon beam is fairly small, and consequently depositing on large area substrates is challenging. Therefore, PLD is almost entirely used for research purposes, that is to develop and study new materials on a small scale. An example of this is the development of the YBa₂Cu₃O₇ high T_c superconductors which were deposited using pulsed excimer laser evaporation (Dijkkamp *et al* 1987), and is currently the dominant commercial application of PLD. The advantage of PLD for this application is the possibility of a stoichiometric transfer of multielement compounds from a single target to the substrate that is achieved for (some) complex materials.

PLD has been discussed in a number of review articles through the years (Cheung and Horwitz 1992, Cheung and Sankur 1988, Fujioka 2015, Shen *et al* 2004, Willmott and Huber 2000) as well as in books such as Eason (2007).

2.5. Other evaporation-based PVD techniques

Molecular beam epitaxy (MBE) is a thin film deposition technique in which thermal beams of atoms or molecules are directed toward a single crystalline substrate, that is maintained at high temperatures, in order to grow epitaxial film, while the deposition process is performed under ultrahigh vacuum (UHV) conditions. MBE is based on evaporation of pure elemental species from resistively heated sources forming localized beams of atoms or molecules which are the source of the constituents of the growing film. The elevated substrate temperature provides sufficient thermal energy to the arriving atoms to migrate over the surface to lattice sites. The evaporation sources are referred to as Knudsen cells. The design and operation of the MBE deposition sources are discussed by e.g. Bean (1993) and Knodle and Chow (2002). The clean environment, the slow growth rate as well as independent control of the beam sources enables precise fabrication of films and stacked structures.

The MBE systems are typically "baked out" (heated) at 150 °C–250 °C and therefore the deposition species must have negligible vapor pressures at these temperatures, which prevents the use of unusually high vapor pressure elements. Also, elements with very low vapor pressure such as silicon, carbon or boron, may require source temperatures well above 1000 °C. At these temperatures there is generally significant co-evaporation of heater or insulator elements, contaminating the intended flux. The evaporation is therefore typically limited to those elements that sit within the center region in vapor pressures (see figure 4). The deposition of low vapor pressure elements such as Si and Ge therefore calls for use of electron beam evaporation (or e-gun) sources. For the deposition of III–V semiconducting nitrides, a radical plasma source, that provides nitrogen atoms to the process, is needed. This is often a dc hollow cathode discharge, an ECR discharge, or an inductively coupled discharge.

The MBE technique is, in particular, widely used for the growth of epitaxial semiconducting films. A typical growth rate for III–V semiconductors by MBE is on the order of 1–3 ML s⁻¹ (a few monolayers per second), which for GaAs corresponds to roughly to 0.3–1 nm s⁻¹, and is quite low. MBE deposition is therefore almost entirely applied in research environment, to explore novel materials and for the development of electronic and opto-electronic devices. More details on the MBE technique can be found in a number of review articles (Arthur 2002, Cho 1995, 1971, Knodle and Chow 2002, Ptak 2015) and in books (Herman and Sitter 1996, Parker 1985).

Close space sublimation (CSS) sources are often used to deposit thin films, in particular CdTe and CdS thin films for solar cells (Amin and Rahman 2017, Rahman *et al* 2019). Figure 11 shows a schematic view a close-space sublimation apparatus. The source material can be powdered and placed so that it faces the substrate surface. The substrate and source are placed on appropriate holders (often graphite boat), and are separated by a small distance (often 1–5 mm), and enclosed in a fused silica tube with gas inlet and outlet tubes to create a controlled environment. During the deposition period, this is placed inside a furnace and the pressure lowered. The key

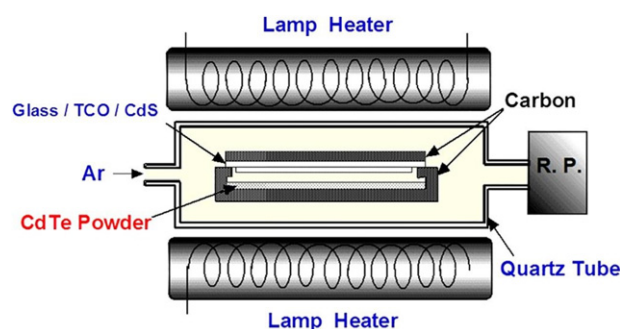


Figure 11. A schematic of the close-space sublimation apparatus. The source material (here CdTe) can be powdered and placed so that it faces the substrate surface. The substrate and source are separated by a small distance, typically 1–5 mm. The substrate and the source material are typically enclosed in a fused silica tube. Reprinted from Rahman *et al* (2019), Copyright (2019), with permission from Elsevier.

process parameters are the temperatures of the source and the substrate, the operating pressure in the reaction tube, and the composition of the source material. Figure 12 shows the temperature schedule for the source material and the substrate, for the deposition of CdTe on single crystalline CdS substrate (Mitchell *et al* 1975). The substrate temperature is raised to the desired deposition temperature a few min before the source temperature reaches its desired value. The source is maintained at a higher temperature than the substrate as demonstrated in figure 12. After the deposition, both the substrate and the source are cooled rapidly. To maintain the desired temperatures, infrared radiation is typically used as a heat source, and thermocouples are inserted into the sample holders to monitor the temperatures. For a given temperature, the sublimation rate increases rapidly as the operating pressure is reduced from atmospheric pressure. At pressures of about 100 Pa, the mean free path of the gaseous species has increased enough, such that the condensation process is no longer limited to the space between the substrate and the source material. The deposition rates can be high; for CdTe films it can be as high as 150 nm s⁻¹ (Amin and Rahman 2017). The operating pressure is typically in the range 100–4000 Pa and the substrate temperature is in the range 500 °C–600 °C, while the source temperature is in the range 700 °C–900 °C (Amin and Rahman 2017). Parameters such as the source temperature and temperature differential are crucial for depositing high-quality films. A fully automated single vacuum manufacturing tool that utilizes multiple inline CSS sources with automated substrate control is described by Swanson *et al* (2016). Plasma-enhanced close-spacing sublimation (PECSS) technique has been demonstrated to improve the efficiency of such devices (Metz 2012, Swanson *et al* 2013, 2011). This approach uses dc hollow cathode discharge to clean the substrate prior to deposition of the active layer.

3. Sputter-based techniques

Sputter deposition has been applied to deposit thin films for over 140 years. For the first 50 years after its practical implementation (Wright 1877) cathode sputtering was mainly

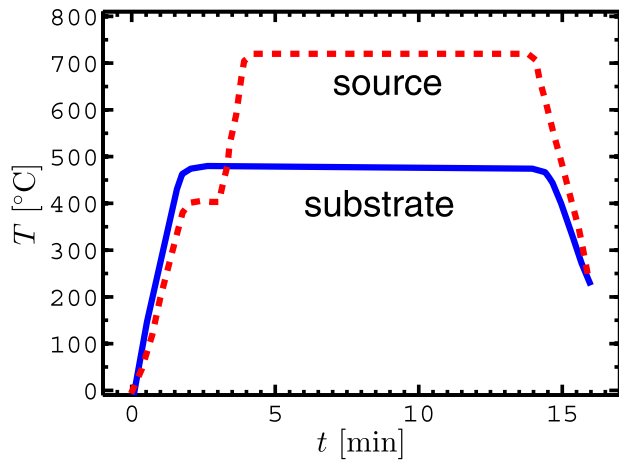


Figure 12. An example of a temperature schedule for the source and the substrate employed in CSS deposition of CdTe on CdS single crystal substrate. Based on data from Mitchell *et al* (1975).

applied for the production of reflecting surfaces on mirrors and prisms (Fruth 1932). With improvements in vacuum technology, sputter deposition yielded to evaporation deposition as the main film deposition technique and it remained so for a few decades. However, sputter deposition regained interest in the early 1960s as a technique for the fabrication of thin films with increasing utilization in various applications. This occurred as it was realized that a wider range of materials, including alloys, could be deposited by sputter deposition rather than by evaporation deposition. In fact, sputter deposition is an effective approach for a controlled deposition of various materials, including alloys and compounds even with complex composition. The main difference to evaporation is the fact that the film-forming species in a sputter process are energetic with energies of a few eV. Sputtering originates from collision cascades of ions impinging onto a target. The sputtered species can leave the target with substantial energy. The energy distribution of the sputtered species follows a Thompson distribution (Thompson 1968).

In sputter deposition, the source of ions for the sputter process is typically a glow discharge, which is a very cost-effective source of ions. The preferred ions for sputtering are the ions of a heavy inert gas. The working gas is most often argon, which is inert, and relatively inexpensive. Such a discharge is typically formed between two parallel electrodes where the cathode and the anode are separated by a distance of a few cm. The gap between the electrodes is filled with the working gas at pressure p_g . A voltage is applied between the electrodes. This can be simply a dc voltage or some periodic waveform. If the voltage V_D is maintained above a certain minimum, the discharge is self-sustaining. In a dc glow discharge, almost the entire applied voltage drops across the cathode sheath or the cathode dark space, that develops next to the cathode, and the ion bombarding energy can be comparable to the value of the applied voltage. The ions created within the discharge are accelerated across the cathode dark space, toward the negatively biased cathode. The bombardment of the electrode by the ions of the inert working gas releases electrons from the cathode, the secondary electrons. These electrons are

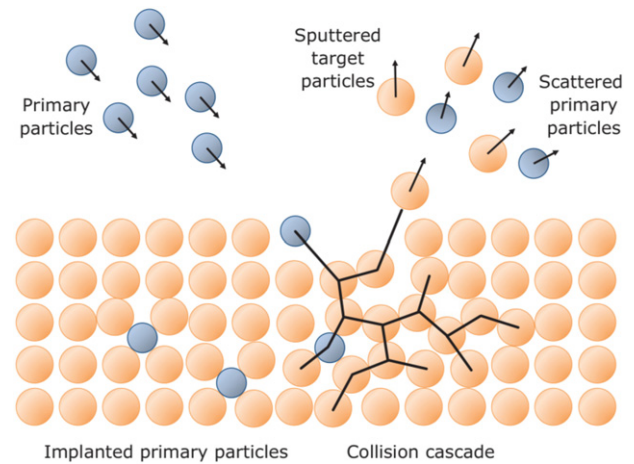


Figure 13. A schematic showing selected fundamental processes that occur due to ion bombardment of a solid target. Reprinted from Bundesmann and Neumann (2018), with the permission of AIP Publishing.

accelerated across the cathode sheath, away from the negative cathode. They, therefore, gain sufficient energy to excite and ionize the atoms of the working gas, which is the main mechanism that maintains the dc discharge.

3.1. Ion–solid interaction–sputtering

When an energetic particle hits a solid target, the incoming primary particle collides with a target atom transferring energy and momentum. This initiates a number of processes, some of which are shown schematically in figure 13. The scattered primary particle and the recoiled target atom can encounter further collisions, and collision cascades can develop. For discharge voltages typically applied, the incident species has sufficient energy to break bonds and dislodge atoms within the target. The target species can also leave the target, in particular those close to the surface. It is called sputtering when an atom is ejected from a solid (or a liquid) due to bombardment by energetic particles, often ions. When the target species gain enough energy in order to overcome the surface binding energy \mathcal{E}_{sb} they can be sputtered, which can be due to a single collision (direct sputtering) or as a result of multiple collisions (collision cascade). The primary species can either leave the target (scattered species) or they can become implanted in the target. As the sputter process progresses the implanted primary particles can be sputtered or they can outgas from the target.

Lets assume that the incident energetic particles are ions. Depending on the energy of the incident ions \mathcal{E}_i and the mass ratio of the projectile and the target atoms M_i/M_t , the collision cascade can proceed as (i) a single-knock-on cascade, (ii) a linear cascade, and (iii) a spike cascade (Greene and Barnett 1982, Mahieu *et al* 2008, Sigmund 1969). In the single-knock-on cascade, the incident species transfers energy to the target atoms, after undergoing a few one-to-one collisions, which are then ejected from the surface. In the linear and spike cascade processes, a cascade of recoils is generated, causing ejection of atoms from the surface. The typical sputter processes fall into category (i), and in particular magnetron sputtering falls in the lower energy part of the linear cascade process.

The sputter process is described by the sputter yield $Y(\mathcal{E}_i, \theta_i)$ which is defined as the mean number of atoms removed from a target surface for each incident ion, and depends on the energy of the incident ion \mathcal{E}_i , the angle of incidence θ_i , the ion mass M_i , and the surface binding energy of the target material \mathcal{E}_{sb} . Various empirical formulas for the sputter yield as a function of ion bombarding energy and data for various combinations of bombarding ions and target materials are given by e.g. Yamamura and Tawara (1996) and/or Eckstein (2007). The sputter yield for a given impacting species on a given target, as a function of the energy of the incident particle, can also be calculated using computer codes such as TRIM (Transport of Ions in Matter) (Biersack and Haggmark 1980), SRIM (Stopping and Range of Ions in Matter) (Ziegler *et al* 2008, 2010) and TRIDYN (A TRIM simulation code including dynamic composition changes) (Möller and Eckstein 1984, Möller *et al* 1988).

The atoms that are ejected from the cathode target have considerable energy, and the sputtered neutrals exhibit a broad energy distribution which is described by the Thompson random collision cascade model (Thompson 1968, 1981) and often referred to as the Sigmund–Thompson distribution function and approximated by

$$f_{S-T} \propto \frac{\mathcal{E}_t}{(\mathcal{E}_t + \mathcal{E}_{sb})^{3-2m}}, \quad (12)$$

where \mathcal{E}_t is the energy of the target species, \mathcal{E}_{sb} is the surface binding energy of the target material and m is the exponent in the interaction potential applied $V(r) \propto r^{-m}$ (Hofer 1991). This model describes an energy distribution that peaks sharply at $\frac{1}{2}\mathcal{E}_{sb}$, followed by a gradual decrease to higher energies ($\propto 1/\mathcal{E}_t^2$). The Sigmund–Thompson energy distribution function, given by equation (12), slightly overestimates the probability to sputter-eject energetic atoms. A modified distribution function was introduced by Stepanova and Dew (2004), where a cutoff energy \mathcal{E}_{max} was added to better reflect experimentally measured profiles

$$f_{S-D} = f_{S-T} \left[1 - \left(\frac{\mathcal{E}_t + \mathcal{E}_{sb}}{\mathcal{E}_{max} + \mathcal{E}_t} \right)^n \right]. \quad (13)$$

Typical values of the constants are $n = 1$, $m = 0.2$ (Stepanova and Dew 2004), and $\mathcal{E}_{max} = 20$ eV (Lundin *et al* 2013). Since \mathcal{E}_{sb} is typically in the range 3–6 eV, most sputtered atoms are emitted with energy in the range 1.5–3 eV.

The ejected atoms exhibit an angular distribution that depends on the direction of the incoming particles. Yamamura *et al* (Yamamura 1981, Yamamura *et al* 1991) give equations for the angular distribution of sputtered species due to ion bombardment under normal incidence

$$\Theta(\mathcal{E}_t, \theta_t) \propto \cos \theta_t (1 + B \cos^2 \theta_t), \quad (14)$$

where B is a fitting parameter that defines the shape of the angular sputter distribution. A cosine distribution corresponds to $B = 0$, while $B > 0$ and $B < 0$ describe angular distributions of over-, under-cosine, and heart-shaped types, respectively. A more thorough discussion on the ion energy and ion angular distribution of the sputtered species can be found in

the reviews given by Hofer (1991) and Gnaser (2007) or the original work of Thompson (1968, 1981) and Sigmund (1969).

3.2. Diode sputter devices

The dc diode sputter discharge is composed of a cathode target placed within a vacuum chamber connected to an external high voltage power supply. The negative applied voltage is often in the range 2000–5000 V. The negatively biased cathode is typically electrically isolated from ground and the grounded chamber often serves as the anode. The substrate, on which the film is deposited, is placed on a substrate holder or substrate table. This discharge arrangement was used as a sputter source for decades, commonly referred to as diode sputtering or cathodic sputtering (Kay 1962, Vossen and Cuomo 1978, Westwood 1976). Figure 14 shows a cross section of a dc diode sputter tool that consists of a sputter fixture (the cathode target) and a concentric substrate table that sits inside a metal cylinder with a shutter located in between. A bias can be applied to the substrate table, but the substrate table can also be electrically floating. The distance between the cathode and the substrate holder is generally short and these discharges are often configured as low aspect ratio discharges, as the inter-electrode separation is small compared to the size of the cathode. Cathode diameters are typically in the range 10–30 cm while the spacing between the cathode and substrate holder is 5 to 10 cm. Almost all the applied voltage appears across the cathode sheath (cathode dark space or the cathode fall). Consequently, the power applied to the discharge is almost completely used to accelerate the ions across the cathode fall to the cathode target. Ion bombardment of the cathode ejects atoms in addition to emission of secondary electrons. The ejected atoms of the cathode material constitute the film-forming material. Due to the bombardment by ions the cathode target heats up and therefore it is desirable to cool the cathode with cooling fluid. The cathode fall is followed by the negative glow, a plasma composed of equal numbers of electrons and ions. The negative glow extends almost to the anode and the positive column is commonly absent. However, a short anode zone where the slightly positive plasma potential returns back to zero at the anode, is present. This configuration is referred to as an obstructed abnormal dc glow discharge. A detailed and practical description of a dc diode sputter device with substrate bias capability is given by Vossen and O’Neill (1968).

The dc sputter source forms a weakly ionized discharge that is dominated by collisions between the neutral atoms. Some of the energetic secondary electrons can pass through the discharge without colliding with an atom and are lost to the substrate or the chamber walls. Therefore, they do not create new ions nor electrons that maintain the discharge but instead cause substrate heating. Consequently, the working gas pressure must be high enough that the secondary electrons are not lost to the grounded surfaces before performing ionization. However, at these pressures the sputtered atoms experience scattering by the working gas atoms. Hence, there is a narrow pressure range around 2–4 Pa for dc glow discharge sputtering to be viable. At this operating pressure, the cathode dark space extends about 1–2 cm from the cathode, while the ion-neutral

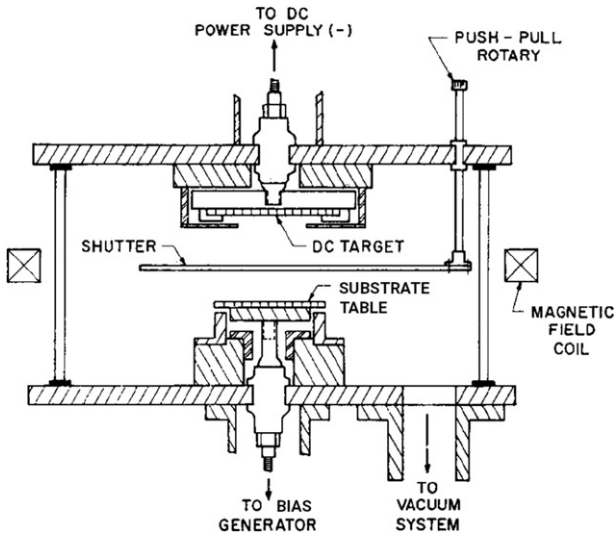


Figure 14. A cross section of a dc sputter diode discharge which allows for substrate bias. Reprinted with permission from Vossen (1971). Copyright 1971, American Vacuum Society.

mean free path $\lambda_i < 1$ cm. Consequently, the cathode sheath is collisional and the ions that impinge on the target surface do not have the full cathode potential and instead exhibit a broad energy spectrum as they bombard the target surface. In principle, sputtering is a line-of-sight process. However, the atoms that are ejected from the target surface, the sputtered species, typically have energies of a few eV but, due to repeated scattering events, they eventually thermalize with the surrounding working gas. Therefore, the sputtered species do not have the excess kinetic energy that is known to be beneficial to the growing film.

3.2.1. Deposition of dielectrics. For the application of dc diode sputtering the cathode target has to be electrically conductive, and therefore, it is mainly applicable for sputtering of metals. If the cathode is itself an insulator, or if the cathode is under operation in reactive gas such as oxygen, which might make the surface of the cathode insulating, an ac voltage at high frequency can be applied to the target (Anderson *et al* 1962, Davidse and Maissel 1966, Logan 1990). Often, these discharges are operated at 13.56 or 27.12 MHz. Due to their lower mass, the electrons are able to respond to the temporal variation of the electric field, while the more massive ions remain mostly stationary. The more mobile electrons are repelled for most of the radio frequency (rf) cycle leading to a positive space charge in front of all surfaces. As there is no dc path through the insulating electrode, the time-averaged flow of electrons and ions to the electrode during each rf cycle must be equal to preserve charge neutrality. To preserve overall charge neutrality, a time-averaged negative charge accumulates on the surface of the insulator (the target). The electrons, due to their high mobility, can provide enough charge over just a fraction of the rf cycle to neutralize the positive ion charge

which flows during most of the rf cycle. Therefore, a nearly steady state saturated ion current flows during most of the rf cycle except near the positive maximum, when an electron current replenishes the negative surface charge, that was lost during the remainder of the rf cycle. The target surface voltage is positive for only a very small fraction of the rf cycle (Logan 1990) while the ion bombardment of the cathode target is almost continuous. This is illustrated in figure 15(a) where the target surface voltage becomes positive at $t/T = 1/4$ and by figure 15(b) showing the replenishing electron pulse. Consequently, the plasma potential is more positive than the potential of the electrodes. In addition, the sinusoidal voltage on the target surface may also be superimposed by a negative dc value with a mean value known as the dc-offset voltage. This dc-offset value depends either on the geometric asymmetry of the reactor, namely the area ratio between the powered electrode to the grounded electrode, or in some cases to the exact waveform of the applied rf-signal that may induce an electrical asymmetry in an otherwise geometrical symmetric electrode assembly. This dc self-bias is zero for a simple sinusoidal rf voltage and identical sizes of powered and grounded electrodes or it can reach up to half of the rf amplitude for a very small powered electrode and a large grounded surface area. In diode sputtering, the latter is typically the case. Figure 16 shows a model of a voltage driven geometrically asymmetric capacitively coupled rf discharge. The dc self-bias follows from rf current conservation through the plasma that depends on the charging and discharging of the capacitance of the cathode target (C in figure 16). The dc self-bias voltage builds up such that the voltage $V(t) = V_b(t) - V_a(t)$ across the discharge can be written

$$V(t) = V_{rf} \sin \omega t - V_{bias} \quad (15)$$

where V_{rf} is the amplitude of the applied sinusoidal voltage. The self-bias that builds up is given by (Chabert *et al* 2021, Lieberman and Lichtenberg 2005, section 11.5)

$$V_{bias} = T_e \left(\frac{1}{2} \ln \left(\frac{M}{2\pi m_e} \right) + \ln I_0(V_{rf}/T_e) \right) \quad (16)$$

where I_0 is the modified Bessel function. For the case when $V_{rf} \gg T_e$ the modified Bessel function can be approximated by

$$I_0(V_{rf}/T_e) \approx \left(\frac{T_e}{2\pi V_{rf}} \right)^{1/2} \exp(V_{rf}/T_e) \quad (17)$$

so equation (16) becomes

$$V_{bias} = V_{rf} + \frac{T_e}{2} \left(\ln \left(\frac{M}{2\pi m_e} \right) - \ln \left(\frac{2\pi V_{rf}}{T_e} \right) \right) \quad (18)$$

which to a zero-order gives $V_{bias} \approx V_{rf}$. This value is increased by the thermal term and is decreased since the electrons reach the electrode only over a finite time interval. This result applies to the driven cathode sheath for a highly asymmetric discharge with small powered electrode (the target) and large grounded counter electrode (or chamber walls).

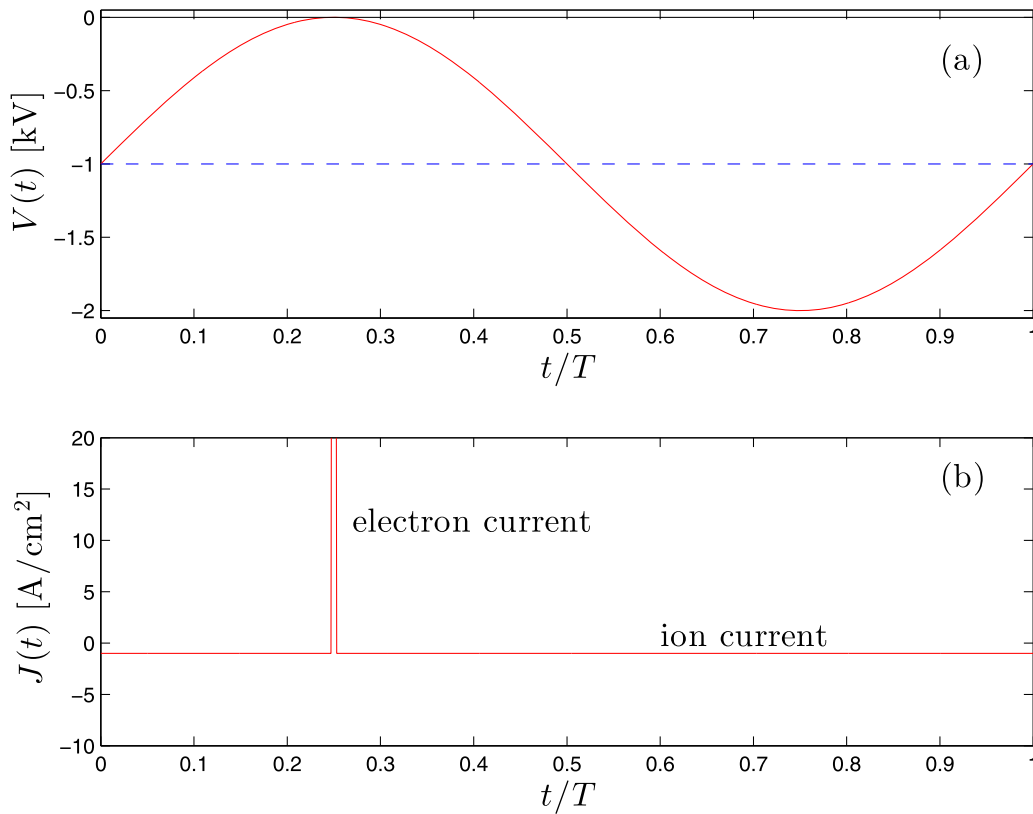


Figure 15. The (a) voltage waveform across the discharge and (b) the current density at an rf plasma boundary.

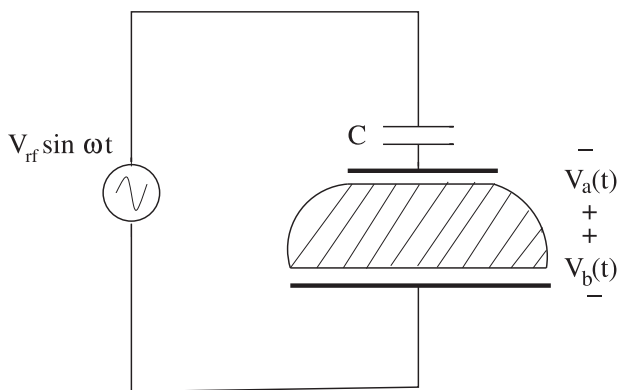


Figure 16. A schematic of the geometrically asymmetric rf diode sputter tool. Based on Kawamura *et al* (1999).

3.2.2. Deposition rate. The rate at which the film-forming species are sputtered off the cathode target depends on the flux, type and energy of the incident particles, the working gas ions as well as the target material. The sputter rate is proportional to the discharge current when the applied voltage is kept fixed. The maximum achievable discharge current density is roughly 1 mA cm^{-2} and the deposition rate 0.2 nm s^{-1} at best. Furthermore, the sputter power efficiency (sputtered atoms/ion-volt) is low in these discharges. Note that rf sputtering can be performed at lower working gas pressures ($<1 \text{ Pa}$) than is viable for dc diode sputtering. However, the sputter rate is very low as dielectrics can have sputter yields as low as one tenth of those of metals. The low deposition rate is a significant drawback to these tools.

The advantage of diode sputtering is efficient use of the target material as the ion flux is nearly uniform across the target surface, and the electrode area does not need to be planar. Sometimes an independent source of electrons is added in order to sustain the discharge rather than relying entirely on the generation of secondary electrons by ion bombardment of the cathode target. This can be achieved by adding a thermionic emitter (e.g. a heated filament). Then the process is referred to as triode sputtering. In the triode arrangement, a dc sputter discharge can be operated at working gas pressure as low as 0.2 Pa . Due to the low deposition rate the dc diode sputter discharge is no longer employed in industrial settings, but discussed here for educational and historical purposes.

3.3. Magnetron sputtering discharges

A magnetron sputtering discharge is a magnetically enhanced diode sputter tool. It is based on magnetically trapping electrons in the cathode vicinity. This is typically achieved by placing permanent magnets near the back of the cathode target. This method is usually referred to as dc magnetron sputtering (dcMS) when driven by dc voltage or current source. A schematic of a circular planar magnetron magnet assembly, including the magnets and the cathode target, is shown in figure 17. The magnetic field lines arch, from a center magnet to an outer magnet ring, above the target surface. The various magnetron sputtering configurations typically utilize a static magnetic field in the range $\sim 20\text{--}50 \text{ mT}$. The relatively weak magnetic field confines the electrons near the cathode target surface while the ion trajectories are not directly

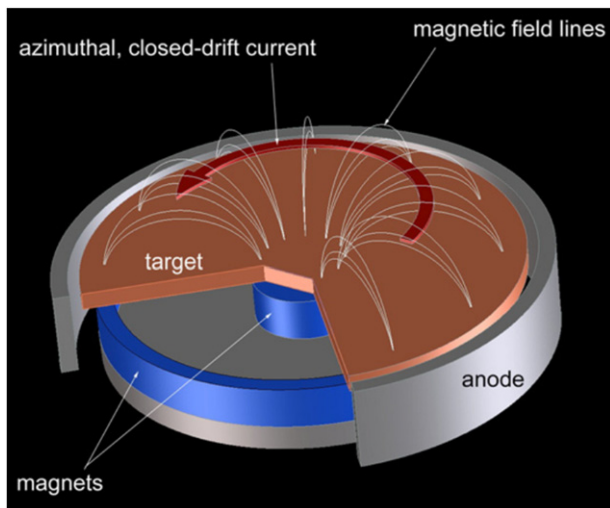


Figure 17. A schematic of a circular planar magnetron magnet assembly, the magnets, the anode, and the cathode target. The magnetic field lines arch, from the center magnet to the outer magnet ring, above the target surface. The magnetic field \mathbf{B} is radial and the electric field \mathbf{E} is axial (along the z axis) and the $\mathbf{E} \times \mathbf{B}$ drift path is azimuthal above the cathode target surface and the resulting azimuthal current. Reprinted from Anders (2011), Copyright (2011), with permission from Elsevier.

influenced (Krüger *et al* 2018). This creates a situation where the electrons are magnetized, while the ions are not magnetized. The electrons follow a bouncing motion along the magnetic field lines \mathbf{B} and also experience the electric field \mathbf{E} from the applied target voltage. As a result, electrons move with an $\mathbf{E} \times \mathbf{B}$ drift along a torus in azimuthal direction as illustrated in figure 17. The confinement of electrons and of ions, however, remains still coupled, because any local deviation of ions with respect to the electrons, being bound to the magnetic field lines, induces electric fields that also confine the ions.

Due to the magnetic confinement of the electrons, the discharge voltage is lowered, the working gas pressure can be decreased, and the deposition rate is increased substantially, compared to non-magnetized dc diode sputtering (Chapin 1974, Waits 1978). The magnetron sputtering discharge is typically operated at working gas pressure in the range 0.1–1.5 Pa and with dc cathode voltage of 300–700 V. These are significantly lower values for both the working gas pressure and the discharge voltage than those required to operate a diode sputter tool and discussed in section 3.2. When operating with dc voltage or current source the resulting current densities are in the range 4–60 mA cm⁻² and power densities are several tens of W cm⁻² (Waits 1978) and the electron density in the substrate vicinity is typically in the range 10¹⁵–10¹⁷ m⁻³ (Gudmundsson 2020). The static deposition rate can be up to 10 nm s⁻¹. However, in dc operation the film-forming material constitutes almost only neutral atoms and the degree of ionization of the sputtered material is generally very low, often on the order of 1% or less, and the majority of the ions bombarding the substrate are ions of the working gas.

The presence of a transverse magnetic field enables a potential drop to exist outside the cathode sheath, the region of dense plasma in the vicinity of the cathode target, the ionization region (IR) (Bradley *et al* 2001, Bultinck and

Bogaerts 2009, Kolev *et al* 2005). The discharge voltage thereby falls over both the cathode sheath and an extended pre-sheath or the ionization region, i.e., $V_D = V_{SH} + V_{IR}$, where V_{SH} is the sheath potential and V_{IR} the potential drop across the ionization region. Unlike non-magnetized dc diode sputtering discharges, which are primarily maintained by ion-induced emission of secondary electrons accelerated in the cathode sheath (Gudmundsson 2020, Gudmundsson and Hecimovic 2017), the presence of a magnetic field leads to a potential V_{IR} across the IR which enables Ohmic heating of the electrons (Brenning *et al* 2016), and describes locally absorbed power by the electrons within the IR. Ohmic heating accounts for a significant fraction of the electron power absorption in dcMS discharges, while it is believed to be the dominating electron power absorption mechanism in high power impulse magnetron sputtering (HiPIMS) discharges (Brenning *et al* 2016, Huo *et al* 2017, 2013). For discharges with a higher fraction of Ohmic heating over total electron heating (Ohmic heating plus sheath energization), the same discharge current can be maintained at a lower discharge voltage, as the discharge becomes more energy efficient (Rudolph *et al* 2022).

The main advantage of magnetron sputtering among the PVD techniques is that the microstructure and properties of the deposited film or coating can be controlled by low-energy ion bombardment during the deposition process. This allows one to control the reactivity and kinetics of the film-forming species and to vary the micro- or nanostructure of the deposited materials, their phase composition, grain size and orientation, density, and internal stress. Magnetron sputter deposition techniques are currently the most widely used processes for thin film deposition and surface engineering treatments. The applications span from thin metal layers in microelectronic circuits, protective layers on cutting tools, to optical films on architectural glass that can be few square meters in size. Depending on the application the magnetron sputtering discharge exists in a number of configurations and various power sources are utilized as discussed in the following subsections. A more detailed discussion of the magnetron sputtering discharge is given in a recent review (Gudmundsson 2020) and an earlier review with a more industrial emphasis by Kelly and Arnell (2000).

3.3.1. Magnetron sputtering discharge configurations. In the 1960s, experiments were conducted where a radially symmetric quadrupole magnetic field was superimposed onto an abnormal glow discharge, which gave a significantly increased ion current density at the cathode (Kay 1963). The early experiments lead to construction of sputter sources that were comprised of two coaxial cylinders. These were either cylindrical-post (the cathode is the inner cylinder and the anode the outer cylinder) (Wasa and Hayakawa 1967a, 1967b, 1969) or hollow cathode or inverted (the cathode is the outer cylinder and the anode the inner cylinder) (Gill and Kay 1965, Thornton and Penfold 1978) magnetron sputter sources. The static magnetic field was then superimposed along the axis of the discharge, transversely to the electric field (radial) which maintains a glow discharge between the electrodes. This creates an electron trap where the electron $\mathbf{E} \times \mathbf{B}$ drift currents close on

themselves. The magnetic field is made strong enough to confine the electrons but not the ions. Despite being important for the development of magnetron sputtering, the cylindrical configurations are not in much use today.

The planar magnetron sputtering configuration was introduced in the early 1970s (Chapin 1974, 1979). The core of the magnetron sputtering discharge in the planar configuration is the magnetron magnet assembly, shown in figure 17. The magnetron magnet assembly is composed of the cathode target and an array of static magnets or electromagnets. In the planar configuration the cathode target is a circular disk or rectangular plate. The magnets are arranged such that a central magnet forms one pole and a magnet ring or a ring of magnets placed along the edge of the cathode target forms the second pole, as seen in figures 17 and 18. The cathode target and the magnets often sit on a water-cooled block of solid copper to prevent overheating. The planar configuration is often used in laboratory settings, with a small circular cathode target, typically 5–15 cm in diameter. In this planar circular magnetron configuration, the static magnetic field is arranged in such a way that the electrons drift azimuthally. Due to the magnetic confinement of the electrons, an intense plasma is concentrated as a donut or a torus-shaped ionization region that sits above the target. Consequently, the plasma is not uniform over the cathode target. The ions originate from this non-uniform plasma region and bombard the target, and the ion current density is peaked and maximum ion bombardment occurs over the region where the magnetic field is tangential to the cathode surface (Wendt 1988, Wendt *et al* 1988). Therefore, a characteristic erosion groove forms in the target surface, referred to as the racetrack (Chapin 1974, Nakano *et al* 2017). The erosion groove determines the target utilization, the target lifetime, and the efficiency of the material usage and is therefore a major drawback of the planar magnetron arrangement in comparison to dc diode sputtering. Typically, the target utilization is below 30% for planar targets. For industrial applications utilizing the planar configuration, the cathode targets are often linear (rectangular), and larger, up to meters long. A prominent example are linear planar magnetron sputtering discharges to deposit thin ceramic heat insulation layers on architectural glass panes with a substrate size of 3 m × 6 m. Here, the glass panes are guided on a conveyor belt underneath a 3 m long rectangular magnetron assembly.

For deposition on large area solar panels, architectural glass, and display panels, large cylindrical cathode targets, as shown in figure 19(a), are commonly utilized. This configuration is referred to as rotatable cylindrical magnetron sputtering. The magnet assembly is installed inside the cylindrical cathode tube (McKelvey 1982, Wright and Beardow 1986). In this setup the magnet assembly is stationary with respect to the discharge chamber walls, and so is the ionization region, while the cylindrical cathode target rotates. The stationary ionization region formed over two rotating cylindrical cathodes can be seen in figure 19(b). In operation, as the cathode target rotates, it is continuously exposed to the plasma zone resulting in a uniform erosion around 360° of the target surface, and the process is sometimes called fully face erosion. Among the benefits of using rotatable cathodes are longer production runs

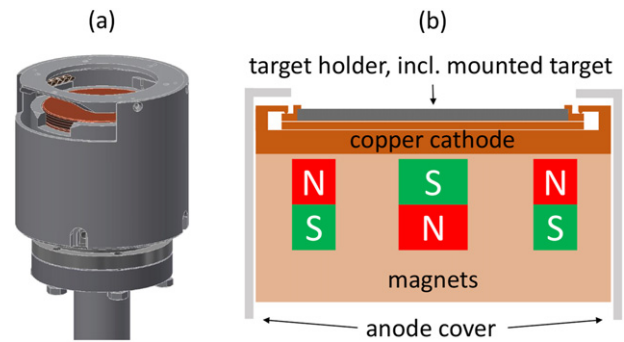


Figure 18. (a) A three-dimensional rendering of a magnetron assembly, and (b) a schematic sketch of the cross-section of the magnetron assembly. Reproduced with permission from L Hayes (2021)

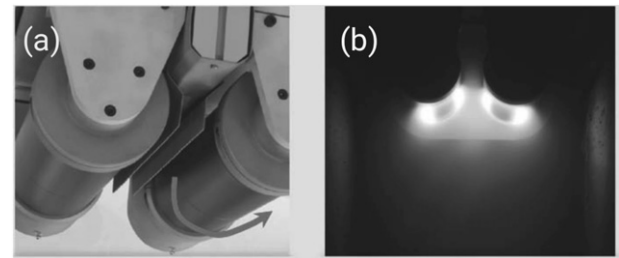


Figure 19. (a) Two cylindrical rotatable cathode targets and (b) the ionization region which is static while the target rotates. Reproduced with permission from Vetushka *et al* (2015) © Copyright 2006–2022, Society of Vacuum Coaters (SVC™).

due to a larger useful target inventory, the target cleanliness, an increased target material utilization, improved target cooling and increased power density, as well as excellent process stability for reactive depositions (Blondeel *et al* 2006). Other advantages of using cylindrical rotating targets is that the thermal load is distributed over the entire circumference of the tubular target instead of a localized heating in the racetrack region in the case of a stationary target. The longer production runs are the results of more target material being available for the sputtering process and due to the rotation, the target utilization is very high and can be higher than 80%. Also, for the rotating cylindrical targets the arching zone is limited to a ring shaped area at each end of the tube, which remains contaminated, as other areas are continuously sputtered and therefore remain clean. This results in reduced machine down time and increased coater throughput. A drawback is that the availability of the target materials tends to be somewhat limited and the cost of the target can be high (Vetushka *et al* 2015).

3.3.2. Magnetic field configuration. As low energy ion bombardment is beneficial for the film properties, one approach to increase the influence of ion bombardment on the film growth was the development of unbalanced magnetron assemblies (Rohde 1994). It is referred to as a conventional or balanced magnetron assembly when all the magnetic field lines that create the magnetic electron trap form closed loops between the magnetic poles as seen in figure 20(a). In reality a perfectly balanced magnetron assembly is not easy to achieve. However, a

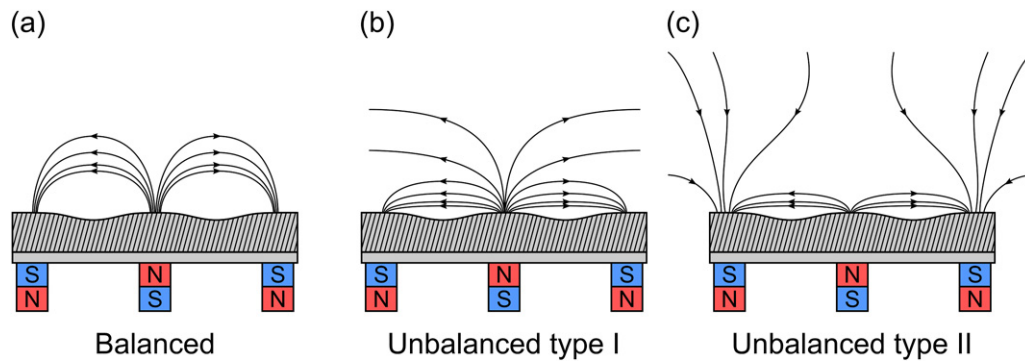


Figure 20. A schematic of the magnet configuration in planar magnetron sputtering discharges. The three cases, (a) all the field lines that originate from the central magnet enter the annular magnet (balanced), (b) all the field lines originate from the central magnet, while some do not enter the annular magnet (unbalanced type I), and (c) all the field lines originate from the annular magnet, and some do not enter the cylindrical central magnet (unbalanced type II). Reprinted from Gudmundsson and Lundin (2020), Copyright (2020), with permission from Elsevier.

perfectly balanced magnetron assembly is not necessarily the optimal magnetic field design, because the unbalanced configuration created by a difference in the strength of the center magnet and the magnets along the periphery of the magnetron assembly allows plasma also to escape toward the substrate. By strengthening the central magnet with respect to the outer magnet, some of the field lines are directed to the chamber walls and the plasma density in the substrate vicinity is low. This arrangement is called unbalanced magnetron assembly of type I (Window and Savvides 1986) and is shown schematically in figure 20(b). When the magnetic field of the outer pole is strengthened relative to the central pole some of the field lines are directed toward the substrate and others are closed between the central and outer magnet poles. Consequently, the electrons can travel toward the substrate region which increases the ionization in the substrate vicinity. This allows ions to reach the substrate, and then by biasing the substrate, the ion bombardment energy can be controlled. This arrangement of the magnetron assembly is referred to as unbalanced magnetron assembly of type II (Window and Savvides 1986) and is shown schematically in figure 20(c).

In order to exploit the magnetron sputtering technology commercially, sputter systems with two or more magnetron assemblies can be arranged to maximize the plasma density in the substrate vicinity. For two magnetron assemblies facing each other it can be either described as ‘mirrored’ (like poles face each other) or as ‘closed’ (opposite poles face each other) field configuration (Sproul *et al* 1990). In the latter case the closing of the magnetic field lines forms a magnetic electron trap that confines the electrons in the region between the cathodes, where the substrate is typically placed. The effect can be further amplified by combining several unbalanced magnetron assemblies into a single system such as the closed-field unbalanced magnetron sputtering (CFUBMS) arrangement, which provides a high plasma density in the substrate vicinity (Kelly and Arnell 2000, Monaghan *et al* 1993). The industrial systems often consist of multiple long rectangular cathodes [even numbers of magnetron assemblies (2, 4, 6, 8)] that surround rotating workpieces. Typically, the magnetic configuration of the neighboring magnetron assemblies alternates to achieve

a joining of the magnetic field lines, in a mirrored closed arrangement. That way the magnetic field lines are linked and maximize the trapping of electrons. Then the losses to the chamber walls are low and the substrate sits in a high density plasma. It has been demonstrated that operation in the closed field configuration results in a significant increase of the ion-to-atom ratio incident on the substrate as compared to a single target unbalanced magnetron, while the deposition rate is not significantly influenced (Kelly and Arnell 1998). On the contrary, in the mirrored arrangement, the field lines are directed toward the chamber walls. In that case some of the energetic secondary electrons follow these field lines and are lost from the discharge, resulting in a low plasma density in the substrate region.

3.3.3. The discharge voltage and current waveforms.

Depending on the application, the applied target voltage can be direct current (dc), radio frequency (rf) or pulsed. This can be achieved by a power, current, or voltage source, depending on the regulation method applied. A particular waveform is selected to avoid instabilities, to provide a high ionization flux fraction of the sputtered species, to allow sputtering from two targets, or to make it possible to sputter from insulating targets. A prominent instability is the so called arcing, which is essentially the onset of an unwanted cathodic arc mode of the discharge, detectable by the appearance of cathode spots and a simultaneous sharp reduction in voltage between the anode and cathode, and sudden rise in the discharge current (Anders 2006). Such instabilities are either initiated by thermionic emission of electrons at hot spots on the cathode surface or by the dielectric breakdown of insulating layers. These extreme events are detrimental for the coating being deposited as well as for the power supplies and need to be avoided. In most commercial power supplies, an arc control is implemented, which temporarily shuts off the power in case of current spikes induced by these arcs.

The dc magnetron sputtering discharge is ideal for depositing thin metallic films from electrically conducting targets. For the deposition from thick electrically insulating (often compound) target materials, rf power needs to be applied. The

discussion in section 3.2.1 on rf diode sputtering, including the formation of dc-self-bias, applies to rf magnetron sputtering (rfMS) as well. As the cathode target is of different surface area than the anode, a dc self-bias develops and is responsible for the ion acceleration through the sheath and onto the cathode target. The dc-self-bias biases the plasma positively with respect to the electrode and appears for all target materials, metallic or dielectric. An important example of the application of rfMS is the deposition of ZnO, a transparent conducting oxide, thin films from a ZnO target (Petrea and Stamate 2021, Stamate 2020). The main advantage of sputtering a ceramic target in this case is the fact that the oxygen atom for film formation is released from the target surface during sputtering and therefore it is easier to achieve stable deposition conditions instead of having to deal with the complications that arise with feedback control in reactive sputtering (see section 3.3.5). A significant drawback for the application of rfMS is that the deposition rate is rather low and the costs of manufacturing ceramic targets through powder metallurgy can be high.

Pulsed magnetron sputtering is utilized in a number of applications. The pulse can be either an asymmetric bipolar pulse or an unipolar pulse depending on the application. One of the most important application of magnetron sputtering is reactive sputtering to deposit compound films such as oxides, nitrides or carbides, in which a metal target is sputtered inside a discharge of reactive gas. Reactive sputtering is a topic of significant importance and will be discussed in section 3.3.5, and is typically performed using asymmetric bipolar waveform. The asymmetric bipolar mid-frequency magnetron sputtering discharge was designed to optimize the deposition of insulating films from conductive targets through reactive sputtering (Sellers 1998). Then the polarity of the target voltage is alternated between negative and positive in each period and the negative voltage pulse amplitude is larger than the positive (roughly 10%–20% of the negative voltage amplitude) voltage pulse amplitude, and there is no off time between the different polarities. A significant portion of each cycle is spent in the sputter mode, and the deposition rate from an asymmetric waveform can approach that of a dcMS. Therefore, asymmetric bipolar magnetron sputtering is sometimes referred to as pulsed dc magnetron sputtering. The asymmetric bipolar waveform is applied to prevent arcing on the target surface during the deposition of non-conducting films. The repetition frequency is typically in the medium frequency range (10–250 kHz) when depositing dielectric films (Schiller *et al* 1993, Sellers 1998).

Sometimes symmetric bipolar or mid-frequency alternating current (ac) waveforms are applied for the reactive sputter deposition of oxide coatings from two targets, called dual magnetron sputtering (Este and Westwood 1988, Heister *et al* 2000, Scherer *et al* 1992). The two targets, often placed side by side, are both connected to the same symmetric bipolar pulser. In this arrangement one target serves as an anode for the system, while the other serves as the cathode target. The roles of the targets are switched when the discharge voltage polarity changes, and a clean target takes over as an anode in each cycle. This approach eliminates what is referred to as the disappearing anode problem, which can occur when all surfaces

including the chamber walls become covered with an insulating oxide. This arrangement is often applied when depositing on large area architectural and automotive glass with large rotating cathode targets (Brückner *et al* 2005) as shown in figure 19(a) with two rotating cylindrical targets side by side. The ac frequency is nominally 40 kHz, however, sometimes the frequency is varied between 10 and 100 kHz to adjust the power delivered to the cathode by frequency modulation (Scherer *et al* 1992).

The waveform can also be unipolar high power pulses and then the process is referred to as high power pulsed magnetron sputtering (HPPMS). By pulsing the power to the cathode target with a high peak power density, a high electron density can be achieved. The unipolar pulse can be a single pulse or be composed of a train of pulses, micropulses, the different approaches all fall under the HPPMS umbrella. When the power density is very high and the duty cycle short the process is referred to as high power impulse magnetron sputtering (HiPIMS) (Anders 2017, Gudmundsson *et al* 2012, Kouznetsov *et al* 1999, Sarakinos *et al* 2010). In HiPIMS operation the repetition frequency is low, typically in the range 50–5000 Hz, the pulses are short 10–400 μs , the duty cycle is short or 1%–3%, and the peak power density is high or $p_t > 0.5 \text{ kW cm}^{-2}$. These discharges reach high electron densities and exhibit significant ionization of the sputtered species. When the unipolar pulse shape is modulated, the pulses are longer, and the peak power density lower than in HiPIMS operation, it is called modulated pulse power magnetron sputtering (MPPMS). Pulsing the discharge not only increases the electron density and the ion flux to the substrate, it also increases the average particle energy. Furthermore, the capabilities of the sputter process are enhanced through control of pulse duration, repetition frequency, and duty parameters.

During the initial stage of the pulse in MPPMS operation (a few hundred microseconds) the power level is moderate (similar to dcMS levels), followed by a high-power pulse (lasting a few hundred microseconds up to a millisecond). The resulting pulse is referred to as a macro-pulse. The macro-pulse can be up to 3 ms long, and the repetition frequencies are in the lower end of HiPIMS operation. The macro-pulse is composed of a train of shorter micro-pulses that appear with frequencies in the range of several tens of kHz. The on- and off-times of these micro-pulses, which are typically up to several tens of μs wide, as well as their frequency can be altered within the macro-pulses. Using this approach, varying the micro-pulse frequency and the ‘on’- and ‘off’-times, arbitrary tailored cathode voltage and discharge current waveforms can be created, including what appears to be a multi-step pulse (Chistyakov and Abraham 2009, Hála 2011, Hála *et al* 2012, Liebig *et al* 2011, Lin *et al* 2011). One variation to the power delivery is to apply packets (or macro-pulses) that consist of a sequence of tightly packed micro-pulses whose duration is only a few μs , referred to as deep oscillation magnetron sputtering (DOMS) (Ferreira *et al* 2016, 2014). By varying the oscillation pulse ‘on’ and ‘off’ times, the peak target voltage and discharge current can be tailored. The duration of the macro-pulse in DOMS is 1–3 ms, and the repetition frequency is typically below 500 Hz. For easier comparison the power delivery in dcMS,

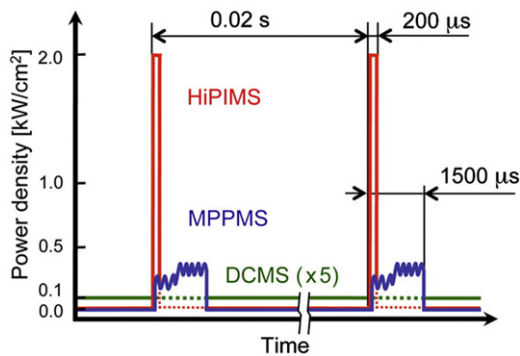


Figure 21. Schematic representation of the power delivery for dcMS and the unipolar pulsed magnetron sputtering discharges HiPIMS ($f = 50$ Hz), and MPPMS ($f = 50$ Hz) when operated at the same average power $\langle P \rangle = 200$ W with 5 cm diameter Nb target. Reprinted from Hála *et al* (2012), Copyright (2012), with permission from Elsevier.

HiPIMS, and MPPMS discharges is shown schematically in figure 21. Over the past few decades there has been substantial development in the design and construction of the pulser units that deliver these unipolar high power pulses as discussed by Hubička *et al* (2020). The pulser units are currently based on insulated-gate bipolar transistors (IGBT) that provide a good control over the pulse length, and have large storage capacitors that maintain the discharge voltage throughout the pulse length.

The goal of the different pulsing schemes is usually to achieve better control over the process and therefore the properties of the deposited films. When the deposition flux contains a high fraction of energetic ions of the sputtered species, it can be utilized to determine the film microstructure. The energy of these ions is a few eV and originates from the sputter process itself, but the energy is also due to acceleration in the plasma sheath in front of the substrate. Furthermore, the ion bombarding energy can be controlled by applying substrate bias (Hubička *et al* 2020). The control of the ion bombarding energy by substrate bias provides control over the E^* axis of the structure zone diagram in figure 3. Such an energetic deposition flux can therefore enable superior film properties due to the enhanced adatom mobility of the condensing species even for deposition at relatively low substrate temperature. Increasing the ionized flux fraction increases the film mass density in the deposited film as was demonstrated by comparing dcMS and HiPIMS depositions for a number of elemental metals (Samuelsson *et al* 2010). Furthermore, increasing fraction of ionization in the deposition flux has influence on the surface morphology, a smoother surface appears as the ionized flux fraction is increased, as can be clearly seen by comparing figures 2(a)–(c). This is indeed observed when comparing the surface morphology of thin films deposited by dcMS and HiPIMS, where the latter deposition method, providing higher ionized flux fraction, results in significantly smoother film surfaces (see e.g. Sarakinos *et al* (2007) and/or Hajihoseini and Gudmundsson (2017)).

However, due to the high ionization degree of the film-forming species in these discharges and as the sputtered neutrals are ionised in close vicinity of the target, they can be

back-attracted by the electric field to the biased target. This is referred to as the return effect (Christie 2005) and it reduces the growth rate per invested power in comparison to dcMS deposition. The resulting low deposition rate is a major drawback to the high power pulse magnetron sputtering technology. In HiPIMS operation, there are two goals: to achieve a high ionized flux fraction of the sputtered target material and to deliver a high deposition rate. The former always comes at the cost of the latter, which is referred to as the HiPIMS compromise (Brenning *et al* 2020). Over the years there have been significant efforts to understand and find ways to alleviate the low deposition rate in HiPIMS deposition. It is well established that the deposition rate depends on the magnetic field strength, and increases with decreasing magnetic field strength (Hajihoseini *et al* 2019, Mishra *et al* 2010). A promising approach has to increase the deposition rate has been to shorten the pulse length (Rudolph *et al* 2020, Shimizu *et al* 2021). It has also been proposed to optimize the HiPIMS discharge operation through mixing two different power levels (Brenning *et al* 2021). Standard HiPIMS pulses create the ions of the film-forming material followed by an off-time, during which no voltage (or, optionally, a reversed voltage) is applied, letting the remaining ions in the magnetic trap escape toward the substrate. After these off-times, a long second pulse with lower amplitude, operated in the dc magnetron sputtering range, is applied (Brenning *et al* 2021, Lou *et al* 2021). During this low power pulse, which is continued up to the following HiPIMS pulse, mainly neutrals of the film-forming material are produced. This pulse pattern makes it possible to achieve separate optimization of the ion production, and of the neutral atom production, that constitute the film-forming flux to the substrate. The low-power pulse is a much more efficient way of creating neutral atoms of the sputtered species to maintain a high deposition rate, while the high power pulse creates ions to a desired predetermined ionized flux fraction. The optimum power split is decided by the lowest ionized flux fraction that gives the desired film properties for a specific application.

The disadvantageous return effect can be mitigated by applying a positive pulse to the sputter target, right after the high power negative sputter pulse, as suggested by Nakano *et al* (2013), (2010), (2014). This raises the plasma potential and accelerates ions out of the ionization region, toward the growing film (Keraudy *et al* 2019). This positive pulse can be few tens to few hundred volts and this approach is referred to as bipolar HiPIMS or HiPIMS with a positive kick pulses.

3.3.4. Instabilities and plasma patterns of magnetron plasmas.

Magnetron sputtering discharges belong to the group of $\mathbf{E} \times \mathbf{B}$ discharges which are known to be subjected to various plasma instabilities. These may be driven by gradients in plasma density, magnetic field, and temperature (Boeuf 2014). Such instabilities have been observed in magnetron sputtering discharges both experimentally and through simulations. Some instabilities may lead to regular moving wave patterns that appear over a wide range of power delivered to the plasma. Examples are high frequency instabilities such as the electron cyclotron drift instability with a traveling pattern with a wavelength in the mm range (Tsikata and Minea 2015) to low frequency

instabilities such as the formation of spokes with a traveling pattern of a region of enhanced ionization with a wavelength of a few centimetres (Brenning *et al* 2013). From an engineering perspective, the occurrence of these instabilities or plasma inhomogeneities are an unwanted aspect for any application. However, the traveling velocity of these patterns is very high, so that any inhomogeneity in the plasma discharge has averaged out in the deposition flux. Moreover, the plasma patterns are also the source of internal electric fields in the plasma that enhance the transport of charged species from the target to the substrate and thereby mitigate the return effect. Note that electron transport across magnetic field lines is governed by instabilities as opposed to classical diffusion. It is generally accepted that instabilities and anomalous transport across the magnetic field lines plays a significant role, however there exist currently no consensus nor real quantification of these phenomena in magnetron sputtering discharges.

Most prominent of these instabilities are spokes or bright plasma emission zones that move azimuthally along the plasma torus with a specific mode number above the cathode (Anders 2012, Ehasarian *et al* 2012, Kozyrev *et al* 2011). These ionization zones rotate in the $\mathbf{E} \times \mathbf{B}$ direction with velocities in the range of typically 10 km s^{-1} at high target power densities. They were coined spokes due to their similarity with *rotating spokes* observed in Hall thrusters (Janes and Lowder 1966). The velocity of the spokes corresponds to the velocity of a plasma excitation or plasma wave, because they travel slower than the electrons with a velocity of 100 km s^{-1} along the plasma torus (Krüger *et al* 2018, Rauch and Anders 2013), but faster than the ions with a velocity of a few km s^{-1} (Poolcharuansin *et al* 2012). A typical image of a plasma pattern on a rectangular chromium target ($3.5'' \times 10''$) taken with a fast intensified charge-coupled device (ICCD) camera is shown in figure 22 (Preissing 2016). The rotation direction is in the $\mathbf{E} \times \mathbf{B}$ direction at high plasma power and in retrograde $\mathbf{E} \times \mathbf{B}$ direction at low plasma powers (Anders and Yang 2017).

The spoke phenomenon is very dynamic since the discharge current during a HiPIMS pulse strongly varies within each single pulse. In industrial applications, with large rectangular magnetron assemblies elongated spokes appear on the straight parts of the target racetrack, and ‘bunching’ of spokes is observed in the curved parts of the racetrack (Anders and Yang 2017, Bobzin *et al* 2017, Preissing 2016). Such a bunching can be easily explained since the $\mathbf{E} \times \mathbf{B}$ drift velocity scales with $1/B$ and because the velocity of spokes is proportional to this drift velocity they slow down in the corners of a rectangular target where the magnetic field is stronger. The plasma density in a spoke is of the order of 10^{19} m^{-3} . Ions exhibit also very high temperatures in the range of a few eV, due to thermalization of the energetic sputtered metal neutral flux (Held *et al* 2018). The ion energy distribution is dominated by low energy ions, but exhibits a high energy tail. Ions are also ejected sideways with an average velocity that is different in or against the $\mathbf{E} \times \mathbf{B}$ direction (Franz *et al* 2016, Panjan *et al* 2014, Yang *et al* 2015). The ionized flux fraction continuously increases with increasing peak power density up to values close to 80%, indicating film growth by incident ions only at very higher

powers (Biskup *et al* 2018). At the same time, the growth rate per invested power significantly decreases with increasing HiPIMS pulse power due to the return effect close to the target. However, this decrease in the growth rate was mitigated, when spokes form in the HiPIMS discharges. The modulation of the electrical potential in front of the target surface by the rotating spokes has been corroborated by emissive probe measurements by Panjan and Anders (2017) for low power discharges and by synchronised Langmuir probe measurements (Held *et al* 2020) for high power cases. The modulation of the plasma potential due to the presence of a spoke largely removes the electric field in the magnetic trap region pointing toward the target. This mitigates very efficiently the return effect in HiPIMS plasmas. In addition, azimuthal electric fields also induce an anomalous electron transport out of the magnetic trap region and thus enhance the transport of plasma to the substrate. Based on particle-in-cell Monte Carlo collision simulations it has been proposed that the spokes appear due to modified Simon–Hoh instability that evolves into ionization instability and is sustained by local electron power absorption induced by ∇B drift along a double layer (Boeuf and Takahashi 2020a, 2020b).

3.3.5. Reactive magnetron sputtering. Reactive sputtering is the process of sputtering an elemental target in a gas mixture of the inert working gas and a reactive gas (e.g. O_2 , N_2 , CH_4 , etc) to deposit compound films. Compound films can also be deposited by sputtering a compound target. A compound refers to chemical binding between at least two chemical elements where at least one is a metal and the other is non-metal (Strijckmans *et al* 2018). By reactive sputtering a range of compounds can be deposited from a low-cost metal target by addition of an appropriate reactive gas to the noble working gas. This includes hard transition metal nitride based coatings, transparent conductive oxides, dielectric layers and photo-catalytically active layers. Reactive magnetron sputtering is therefore of significant industrial and technological importance as the majority of commercially important thin films and coatings are compounds (Kelly 2011). Such coatings are typically deposited by reactive magnetron sputtering using asymmetric bipolar mid-frequency, rf or unipolar pulsed (HiPIMS) waveforms. Reactive sputter deposition is a very important topic and for further details the readers are referred to a recent tutorial by Strijckmans *et al* (2018), a review by Sproul *et al* (2005), and in the context of HiPIMS (R-HiPIMS), a tutorial by Anders (2017).

The sputter yield of the compound material is typically substantially lower than the sputter yield of the elemental target material. Consequently, the deposition rate decreases as the flow rate of the reactive gas is increased and compound is formed on the target surface, and fewer atoms of the elemental target material are sputtered and fewer reactive gas species are consumed. This appears as a sudden and sharp rise in the reactive gas partial pressure and the resulting deposited film becomes rich in reactive gas species. It also indicates that the relationship between the compound film composition and the flow rate of reactive gas is non-linear. Similarly, the deposition rate shows a non-linear dependence on the flow rate of the

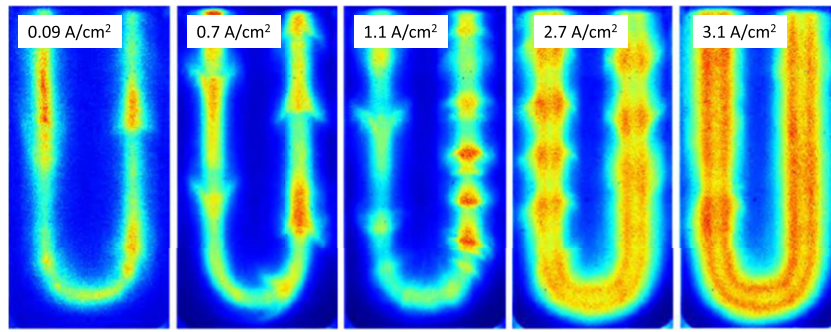


Figure 22. ICCD image of spokes, rotating along the race track above a chromium target ($3.5'' \times 10''$) at different target current densities, as indicated. Reproduced with permission from Preissing (2016).

reactive gas. The difference in sputter yields causes the deposition rate decrease and increase not to occur at the same value of the flow rate of the reactive gas. This shows up as a hysteresis, and the separation width between the decrease and increase defines the width of the hysteresis region. This is shown schematically in figure 23 (from Kubart *et al* (2020)), where the three main operating regions of a reactive magnetron sputtering process are indicated. In the metal mode, all the supplied reactive gas is incorporated into the deposited metal, and the target surface is free of compound. The mass deposition rate increases slightly with increasing reactive gas flowrate up to the point where the deposition rate drops abruptly as a transition from metal to compound mode takes place (seen as seen as a jump from point A to point B in figure 23). Here, all the sputtered metal is converted into compound material, and the excess reactive gas forms a compound layer on the target surface. The deposited films are stoichiometric, and further addition of reactive gas does not have much influence. The compound mode is maintained as the reactive gas flow is reduced until it reaches point C in figure 23. At this point the reactive gas flow is unable maintain the compound layer on the sputter target surface, and a transition to the metal mode (point D) occurs. The presence of hysteresis implies that the transition region A–B–C–D is ill defined. For low reactive gas flows, a metal mode is maintained with predominantly metallic film deposited at a high rate. This also means that it is possible to deposit compound films of different stoichiometries and physical properties at two stable operating states, that correspond to the same value of the flow rate of the reactive gas, within the region of hysteresis. The hysteresis effect is therefore simply due to a competition between two opposing processes: the formation of a compound on the target surface and sputtering of the compound off the target surface. This formation of compound material on the target surface is called target poisoning.

Stoichiometric compound films can be deposited at relatively high deposition rates, if one operates in the transition zone between the metallic and poisoned mode (Sproul 1998). In some cases, a desired stoichiometry at the substrate surface requires an explicit operation of the reactive magnetron process within the transition zone. Therefore, it is important to identify a stable operating point within the transition zone. Early on this control was achieved using mass flow control of

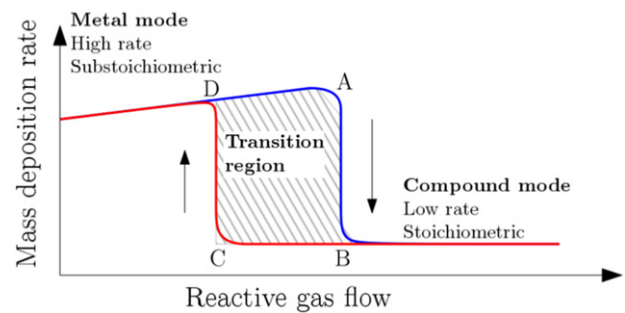


Figure 23. A schematic showing the deposition rate evolution with reactive gas flow. Pronounced hysteresis (wide transition region) defined by the transitions A–B and C–D is shown. Reprinted from Kubart *et al* (2020), Copyright (2020), with permission from Elsevier.

reactive gas into the chamber in attempts to achieve a stable operating point. But this approach leads to operational problems. At fixed power, as the reactive gas flow of the reactive gas is increased, initially all of the reactive gas will be consumed by reaction with metal surfaces, including the cathode target and the chamber walls. Therefore, a number of process parameters change simultaneously when increasing/decreasing the reactive gas flow rate. Furthermore, the precision and speed of the standard pressure gauges (e.g. vacuum ionization gauges) is often inadequate for control of reactive sputter deposition, as their accuracy often depends on the type of gas. It is more practical to determine the operating point by active feedback control of the partial pressure of the reactive gas (Sproul *et al* 2005). This is possible as there is a monotonic relation between the partial pressure of the reactive gas p_{RG} and the target compound fraction θ_t without the appearance of hysteresis. The steady state relation between p_{RG} and the target coverage θ_t is

$$p_{RG} = \frac{J_i Y_{CC} \theta_t}{2\kappa S_{RG} (1 - \theta_t)} \quad (19)$$

where J_i is the ion current density onto the target, Y_{CC} is the partial sputter yield of reactive gas atoms from the compound, S_{RG} is sticking (or incorporation) coefficient, which stands for the probability of a neutral reactive species to bind with a free metal site. Furthermore, the reactive gas flux is proportional to the partial pressure of the reactive gas, and the constant of proportionality is κ . According to equation (19), the partial

pressure p_{RG} is a smooth curve, a function of the target compound fraction. Therefore, the partial pressure is suitable as a control parameter, and the transition between the metal mode and the compound mode is continuous (Sproul 1998).

A feedback control loop requires a precise measurement of the parameter that characterizes the process state. However, direct measurement of partial pressures calls for specialized instrumentation, which is not always available. This can be realized by quadrupole mass spectrometry of the reactive gas species (Sproul *et al* 2005, Sproul and Tomashek 1984), by optical emission spectrometry to detect the sputtered metal species (Schiller *et al* 1987, 1982), or by using the cathode voltage as the feedback signal (Affinito and Parsons 1984). The mass spectrometer provides a direct reading of the particular reactive gas species while the optical emission spectrometry reading and the cathode voltage are indirect measures of the partial pressure.

An optical emission spectrometer can detect an optical emission from metal species that are excited during the reactive sputter process. This signal can be applied in a feedback control loop which is then used to adjust the reactive gas flow rate often through a piezoelectric valve (Schiller *et al* 1987, 1982), an approach that is referred to as a plasma-emission monitor. A monotonic relation exists between the emission intensity of a characteristic line of the sputtered species and the degree of oxidation of the deposited layer. In a reactive sputter process, the metal line intensity exhibits a pronounced drop with increased compound coverage of the target. The increased target coverage is accompanied by a reduction in the ion current onto the target which, consequently, causes a reduction in the metal sputter rate. These optical emission based methods are fast and of relatively low cost.

Note that the pumping speed also plays a significant role. At sufficiently high pumping speeds the hysteresis may be avoided (Kadlec *et al* 1986, Okamoto and Serikawa 1986). The absolute value of such a critical pumping speed, however, can often be unrealistically high and therefore it is often practically unfeasible. Also, it is not economical.

3.3.6. Ionized physical vapor deposition and ionization processes. In a sputter deposition process the sputtered species are released from the cathode target as atoms or molecules. For magnetron sputtering discharges driven by dc, rf and asymmetric bipolar waveforms, the film-forming material at the substrate consists almost entirely of neutral atoms. However, it is often desired to have ions of the film-forming species bombarding the substrate, as it is well established that low energy ion bombardment (E_i is below the lattice displacement threshold, $\sim 20\text{--}50$ eV depending upon the ion and deposited film) in the deposition process, has a significant influence on the deposited film microstructure and the film properties (Petrov *et al* 2003) (see also figure 3). Ionizing the sputtered material has several advantages: improvement of the film quality, deposition on substrates with complex shapes, enhancement and control of the reactivity in the growth process. This influences the crystallite orientation, grain size, the epitaxial temperature, the film mass density, as well as stress in the film (Greczynski *et al* 2019, Greene and Barnett

1982). Bombarding the growing film with ions of the noble working gas can create residual ion-induced compressive stress in the film, while bombarding the growing film with the ions of the film-forming material has several advantages: improvement of the film quality, and improved step coverage and conformity (Greczynski *et al* 2019). Furthermore, by ionizing the sputtered species, the ion bombarding energy at the substrate can be controlled by applying a substrate bias. Additionally, a directional deposition and collimation of these ions with the plasma sheath adjacent to the wafer is made possible. A PVD process where the flux of ions Γ_i is larger than the flux of neutrals Γ_n for the sputtered species, or $\Gamma_i > \Gamma_n$, is called ionized physical vapor deposition (IPVD) (Hopwood 2000). Achieving highly ionized flux of the sputtered material was initially based on the application of a secondary discharge to create a dense plasma between the evaporation or sputter source of the film-forming material and the substrate so that a large fraction of the sputtered atoms are ionized (see section 3.3.7).

The dominating ionization process in IPVD discharges is electron impact ionization, and to ionize the sputtered species the average distance it travels before being ionized has to be reasonably short. The ionization mean free path for electron impact ionization is given by

$$\lambda_{iz} = \frac{v_s}{k_{iz}n_e}, \quad (20)$$

where v_s is the velocity of the sputtered neutral atoms, k_{iz} is the electron impact ionization rate coefficient and n_e is the electron density. In dcMS operation $n_e \sim 10^{15}\text{--}10^{17} \text{ m}^{-3}$ and $\lambda_{iz} \sim 1$ m and the fractional ionization of the sputtered atoms is expected to be low. For $n_e \sim 10^{18} \text{ m}^{-3}$ and λ_{iz} is tens of cm. These are the typical parameters for a IPVD systems based on a secondary inductively coupled plasma (ICP) or ECR discharge. For electron density of 10^{19} m^{-3} , the densities achieved in the HiPIMS discharge, the ionization mean free path is of the order of one cm. The high electron density is therefore the key to achieve a high degree of ionization of the sputtered material. The ionization of the sputtered species is typically given as the ionized flux fraction of species s as (Hopwood 1998)

$$F_{\text{flux}}^{(s)} = \frac{\Gamma_i^{(s)}}{\Gamma_i^{(s)} + \Gamma_n^{(s)}}, \quad (21)$$

where $\Gamma_i^{(s)}$ and $\Gamma_n^{(s)}$ are, respectively, the ion and neutral fluxes of the species s arriving at the substrate or detector. The deposition rates are then recorded by manually recording the film thickness at a chosen time on a readout unit connected to the quartz crystal micro-balance (QCM). The ionized fraction of a metal flux can be determined by measuring the total mass deposition rate and the mass deposition rate of neutral metal atoms only, as discussed by Green *et al* (1997) and Wu *et al* (2010).

3.3.7. Magnetron sputtering with secondary discharge. Various approaches have been taken over the past few decades to increase the ionization of the sputtered species in magnetron sputtering by adding a secondary discharge to create

a dense plasma in the region between the cathode target and the substrate (Helmersson *et al* 2006). These systems consist of a dcMS source and a secondary discharge which could be either inductively coupled (Rosnagel 2000, Rosnagel and Hopwood 1993, 1994, Wang *et al* 1999) or microwave-driven (Musil *et al* 1991, Takahashi *et al* 1988, Xu *et al* 2001) discharges. The secondary discharge creates a dense plasma that ionizes a large fraction of the sputtered species as it passes through. This technique was initially developed to deposit metal layers and diffusion barriers into trenches or vias of high aspect ratio in microelectronic fabrication (Hopwood 1998, 2000, Rosnagel 1999). Other methods of creating highly ionized sputtered material include shaping the cathode target in a particular way in order to confine the electrons, referred to as hollow cathode magnetron sputtering discharge (HCM) (Klawuhn *et al* 2000, Lai 2000).

The inductively coupled plasma (ICP) discharge is driven from a non-resonant induction coil that is placed parallel to the cathode target as shown in figure 24. The magnetron assembly is located on the top of the chamber. The sputtered species transit the dense plasma, created by driving rf current through the inductive coil, where they are ionized (Barnes *et al* 1993, Rosnagel 2000, Rosnagel and Hopwood 1993, 1994). The rf coil is typically located a few cm below the cathode target surface and has diameter that is 20%–40% larger than the substrate diameter (Rosnagel 2000). The inductive coil is often driven at 13.56 MHz using a 50 Ω rf generator through a capacitive matching network. The rf power is typically in the range 200–1000 W resulting in an electron density in the range of 10^{16} – 10^{18} m⁻³, that increases linearly with increased applied rf power (Hopwood 1992, Hopwood *et al* 1993). The ICP-assisted magnetron sputtering discharge is typically operated at rather high working gas pressures, in the range 2–4 Pa, to thermalize the film-forming species which shortens their ionization mean free path (Rosnagel 2000, 1999). The inductively coupled plasma assisted magnetron sputtering (ICP-MS) discharge is still very widely used in the microelectronics industry for deposition of metal films such as conductors, diffusion barriers, and adhesion and seed layers.

A secondary discharge can also be created by adding a ECR discharge in the region between the magnetron assembly and the substrate (Xu *et al* 2001), the cathode target can be placed between the ECR discharge and the substrate (Berry and Gorbalkin 1995, Gorbalkin *et al* 1996, Musil *et al* 1991, Ono *et al* 1984, Takahashi *et al* 1988) or the microwave power can be introduced to the discharge through coaxial-type cavity that surrounds the cathode target (Yoshida 1992). An ECR discharge provides high plasma densities (10^{17} – 10^{18} m⁻³) and the working gas pressures can be low (0.01–2 Pa). The ECR discharge is based on wave absorption and requires application of a strong stationary magnetic field (87.5 mT at resonance) and microwave power (e.g., 2.45 GHz) which is injected as a right-hand circularly polarized wave into a resonance zone. The introduction of a magnetic field leads to a resonance between the microwave frequency (ω) and the electron cyclotron frequency $\omega_{ce} = eB/m_e$ within the discharge. Due to the cyclotron resonance, the gyrating electrons rotate in phase with the polarized wave and the wave energy is absorbed by a

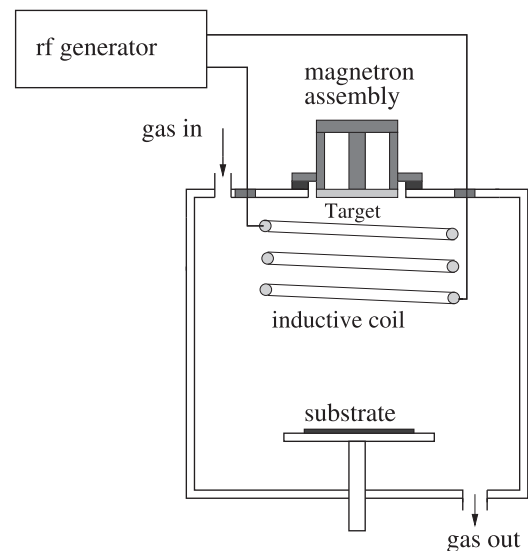


Figure 24. A schematic of an ICP-MS in which a radio-frequency-driven inductively coupled discharge is placed parallel to the cathode target in the region between the cathode and the substrate. Reproduced from Gudmundsson (2020). © The Author(s). Published by IOP Publishing Ltd. CC BY 4.0.

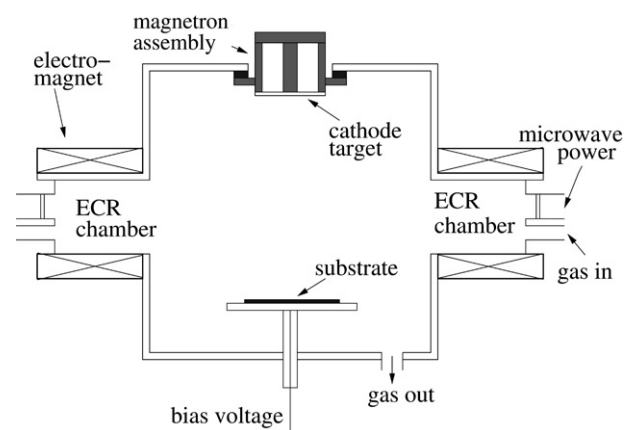


Figure 25. A schematic of an ECR-MS apparatus, two ECR discharge chambers are located at the opposite sites of the main processing chamber. A highly ionized plasma is created in the region between the magnetron sputtering cathode target and the substrate. Reproduced from Gudmundsson (2008). © IOP Publishing Ltd. CC BY 3.0.

collisionless heating mechanism. Figure 25 shows a schematic of an ECR-assisted magnetron sputtering discharge, where two ECR discharges are placed between the cathode target and the substrate. Electromagnets are placed around the periphery of each of the ECR discharge chamber to create magnetic field of 87.5 mT and a resonance zone within each of the chambers.

This IPVD technique has also been demonstrated for ionizing thermally evaporated metal by having it pass through an ECR discharge (Holber 2000, Holber *et al* 1993) as discussed in section 2.1. For sputter deposition systems, based on a secondary high density discharge, it has been reported that a significant fraction of the sputtered species is ionized and that the ionized flux fraction increases with increased power to the secondary discharge. The ionized flux fraction for Cu has been reported to reach values higher than 80% (Rosnagel

and Hopwood 1994). The ions of the sputtered material can subsequently be accelerated toward the substrate to a desired ion bombarding energy by applying a dc bias to the substrate.

3.4. Ion beam sputter deposition

Ion beam sputter deposition is a PVD technique that is used to deposit high-quality thin films. Ion beam techniques are non-thermal techniques in which the energy of the impinging flux is controlled by an electric field. Ion beam deposition offers the opportunity to influence the properties of the film-forming species and consequently the thin film properties can be varied by changing the ion beam and/or geometrical parameters over a wide range. There are two approaches to apply ion beams for thin film deposition (Harper 1978, Rosnagel and Cuomo 1988). The first approach is primary ion beam deposition where the ion beam is composed of the film-forming material which is deposited at low energy (~ 100 eV) directly onto the substrate. The other approach is secondary ion beam deposition where the ion beam is typically composed of ions of an inert gas that are accelerated to high energy (hundreds to thousands of electron volts). This ion beam is then directed at a target that constitutes the film-forming material and the ions of the inert gas sputter the target. These sputtered film-forming species are then collected onto a nearby substrate. In both the ion beam processes the ions are generated at some distance from the substrate and the ion beam is directed onto the substrate or a target. In the latter process the ion generation and acceleration (ion beam source), and the generation of the film-forming species (target), and thin film deposition (substrate) are spatially separated. Typically the geometrical parameters (ion incidence angle and emission angle) as well as the ion beam parameters (ion species and ion energy) can be varied, which influences the energy and angular distributions of the film-forming species, the sputtered target species, as well as backscattered primary species.

The main advantages of ion beam processing are excellent control of the flux and energy of the ions incident on either the substrate or a target (for sputter deposition) and the absence of the "arcing" instability, thus absence of arc-generated particulates. The independent control of the ion energy and the ion flux during the deposition process can be used to modify the film grain size, nucleation density, defects, crystal structure lattice spacing, preferred crystallite orientation, density, and stress. The ion beams applied for thin film materials processing are operated at low background pressures, typically below 10^{-2} Pa, so that both the incident ion beam and the sputtered atoms are a line-of-sight processes. The pressure is kept low enough that collisions with the background gas are rare, and most of the sputtered atoms pass right through.

An ion beam sputtering setup is shown schematically in figure 26. It consists of a broad-beam ion source, a target holder, and a substrate holder. The distance between the exit plane of the ion beam source and the target center and between the target center and the substrates is in the range 10–20 cm. The ion beam source and target holder are typically placed on rotary tables, which have their center of rotation located at the center of the target surface plane. This means that the ion incidence angle α , and consequently the polar emission angle

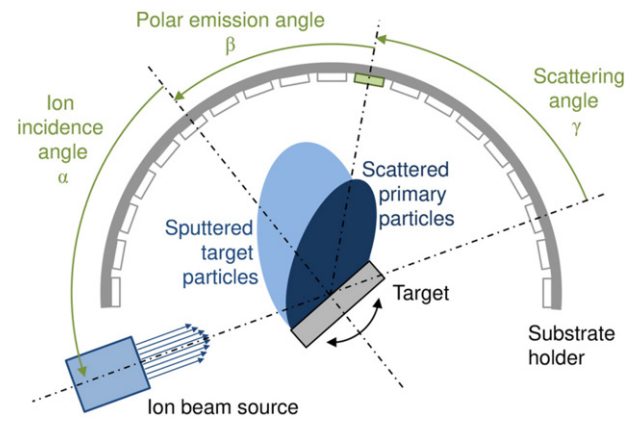


Figure 26. A schematic of an ion beam sputter deposition system. Reprinted with permission from Bundesmann *et al* (2021). Copyright 2021, American Vacuum Society.

β , can be varied. The scattering angle is

$$\gamma = 180^\circ - (\alpha + \beta). \quad (22)$$

Note that the range of feasible scattering angles is somewhat limited. The sputtering and scattering processes can be described by the conservation of momentum and energy in a binary elastic collisions. The ion–solid target interaction and sputtering are discussed in section 3.1.

The ion source is often a gridded broad-beam ion source, sometimes referred to as a Kaufman ion source (Kaufman and Robinson 1989). They are composed of an electrically driven discharge for ion generation and a multi-aperture grid system for ion acceleration and extraction. The discharge can be a rf driven inductively coupled discharge, a capacitive discharge or a microwave driven ECR discharge. One side of the discharge volume has a set of grids or screens. As ions impinge on the mostly open screens, they are accelerated by the applied voltages and leave the source in the form of a broad beam. The grid system is composed of one, two, three, or even four grids. Typically, it is a two- or three-grid system. The first grid (the screen grid) or an auxiliary anode is located inside the discharge chamber. The ions are extracted by applying a negative potential V_{accel} to the second grid (accelerator grid). The absolute value V_{accel} is typically a few hundred volts. Often a third grid (decelerator grid) is added and kept at ground potential. Its role is to prevent electrons of the space-charge-neutralized ion beam to be accelerated 'backwards' into the ion source; such electron current represents an unwanted load on the extractor power supply and causes x-rays, which would then require safety shielding. The resulting ion energy can be in the range from 200 to 2000 eV, the ion current density up to a few mA cm^{-2} , and the total beam power up to several hundred watts.

Ion beam deposition has much lower deposition rate than thermal evaporation or magnetron sputter deposition, as seen in figure 1(b), which is a significant drawback. Furthermore, this technique is not easy to upscale, and in general the ion beam sources are more complex than magnetron sputter deposition systems or evaporation sources. Therefore, ion beam deposition is only applied in niche applications, such as laser

mirror coatings based on dielectric multilayers (Gibson 1987, Stolz and Génin 2003), where the relatively high cost is justified by the superior quality of the resulting films that can be achieved (Bundermann and Neumann 2018).

For further discussion on ion beam deposition the interested reader is directed to the book chapter by McNeil *et al* (2002) and/or the recent tutorial by Bundermann and Neumann (2018).

4. Cathodic arcs

An arc is a discharge of relatively high current (several amperes, often tens or hundreds of amperes, or even higher) at relatively low voltage between electrodes (generally less than 40 V). The operation mechanism of the arc discharge differs significantly from glow discharges used for sputtering. It is characterized by a collective electron emission mechanism. If the cathode is sufficiently hot that the collective mechanism is thermionic emission, one calls this arc a ‘thermionic arc’. In the context of PVD, a different arc mode, the cathodic arc, is much more relevant. Here, the emission of electrons occurs at small (typically micrometer), non-stationary cathode spots based on thermo-field emission: a nonlinear combination of thermionic and field emission (Jüttner 2001). The power density of the cathode spots is extremely high (estimated between 10^{12} and 10^{14} W m⁻²) which leads to evaporation and ionization of the cathode material, and thus to the formation of plasma of the cathode material.

The name cathodic arc is due to the fact that the current-carrying discharge medium between electrodes is the plasma of the cathode material even when gas is present between the electrodes (Anders 2008). A cathodic arc may also burn in vacuum, i.e., without any gas present, and in this case, the arc is known as a vacuum arc (Boxman *et al* 1995). Vacuum arcs are cathodic arcs, but cathodic arcs are not always vacuum arcs since a process gas (or liquid) can be present between the electrodes.

Historically, the name metal vapor vacuum arc was occasionally used, especially in the context of vacuum arc ion sources (Brown 1994). This name is less suitable since it (falsely) suggests the emission of neutral metal vapor from the cathode. In fact, the flux expanding from the cathode spots consists of a fully ionized metal plasma with multiply charged ions (Davis and Miller 1969), a property that will be considered in greater detail below.

Cathodic arcs are prolific sources of plasma of any cathode material. However, in order to serve as a cathode, the material has to be sufficiently conductive to carry the arc current. Pure metals, alloys and sintered metal composites, graphite and highly doped or heated semiconductors have been used as cathode. For example, a titanium cathode delivers titanium plasma. If the operation is in vacuum or in a noble gas like argon, the titanium plasma condenses on any surface, thereby forming a titanium coating. In the context of PVD, one is often interested in compound coatings, such as TiN. In this case, nitrogen is added to the discharge region. To illustrate the versatility of the cathodic arc deposition process: more than one metal can be used in the cathode, or more than one cathode can

be operated, and more than one reactive gas can be added. It is thus possible to readily produce compound films containing multiple elements, for example, TiAlON when titanium and aluminum are in the cathode material, and nitrogen and oxygen are added to the gas. The stoichiometry of the compound can be tuned in a wide range depending on the ion flux ratios arriving at the substrate.

4.1. Plasma from cathode spots

The nonlinear nature of electron emission laws in terms of cathode temperature and electric field leads to spot formation: for the arc discharge to occur, it is energetically preferred to concentrate the discharge power to a very small area on the cathode to obtain the greatest emission of electrons. The current in a vacuum arc discharge is typically concentrated in a luminous area of a few square micrometers on the cathode surface and referred to as cathode spot (Anders *et al* 1996, Jüttner 2001). As a ‘side effect’, the cathode material at these concentration points, the cathode spot, is readily melted, evaporated and ionized. The development of such hot spots is extremely fast (nanoseconds) so that models of wire explosions have been successfully applied to describe the process (Mesyats and Proskurovsky 1989). An example of erosion traces left on a cadmium cathode target after arc deposition due to ejection of fast plasma jets and liquid metal droplets is shown in figure 27. The cathode processes lead to rapid phase transitions and are therefore sometimes referred to as explosive electron emission (Mesyats 1998). The current density has been determined to reach peak values of 10^{12} A m⁻² (Jüttner *et al* 1984) while the plasma density can temporarily reach peak values exceeding 10^{26} m⁻³ (Anders *et al* 1992). At such high densities, the plasma is dense and ‘nonideal’ which, by definition, means that the potential energy between charged particles is not small compared to their kinetic energy. One of the consequences is a reduction of the ionization energy leading to an enhancement of ion charge states (Ebeling and Kilimann 1989).

Arcs in air were studied in the 18th century (Anders 2003, Priestley 1775), while more ‘recent’ studies of their optical spectra, even in the vacuum ultraviolet spectral region, date back ‘only’ a hundred years (McLennan *et al* 1919). The properties of the plasma flux from cathode spots have been extensively studied for decades (see e.g., Boxman *et al* (1995), Davis and Miller (1969), Lafferty (1980), Plyutto *et al* (1965), Tanberg (1930)). Most remarkably, the plasma contains multiply charged ions (most often 2⁺ and 3⁺) that have supersonic speed (relative to the ion sound speed), with Mach numbers between 3 and 5 (Anders and Yushkov 2002). The most likely ion velocity is typically $1-3 \times 10^4$ m s⁻¹. Ion charge state and ion velocity scale with the cohesive energy of the cathode (cohesive energy rule, see Anders (2008) (chapter 3)) which is based on energy considerations of the phase transitions and ionization processes. Also, the discharge voltage is linearly dependent on the cohesive energy \mathcal{E}_{ce} of the cathode material (Anders 2002b, Anders and Yushkov 2002).

The acceleration of positively charged ions away from the (negative) cathode is non-trivial. A combined mechanism

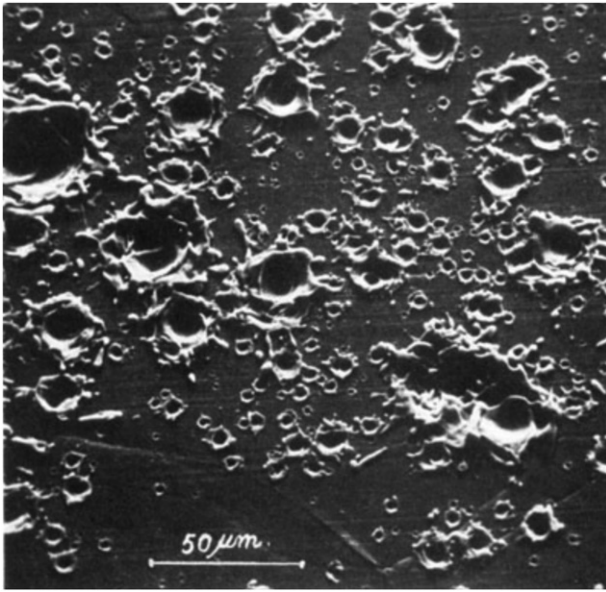


Figure 27. Erosion traces left by a 10 A vacuum arc on a cadmium cathode. Reproduced from Daalder (1979). © IOP Publishing Ltd. All rights reserved.

based on strong pressure gradients and the local electric field of expanding plasma is responsible. One should keep in mind that even for dc (continuous) cathodic arcs, the cathode processes are essentially pulsed due to the non-stationary, even explosive processes. A good picture is to consider the plasma flux as the result of a rapid sequence of microexplosions, thus the plasma flux is pulsating or fluctuating in flux density, ion charge state and velocity (Anders *et al* 2005). Detailed analysis showed that the fluctuations do not show characteristic frequencies but a broad spectrum. This applies to vacuum arcs (Oh *et al* 2021a, Smeets and Schulpen 1988) and also to cathodic arcs in the presence of reactive gases (Oh *et al* 2021b). Figure 28 illustrates the non-stationary, fluctuating character of cathode spot activity and related cathode plasma production. In fact, many of the fluctuating properties (voltage, current, ion current, charge states, etc) follow a power law with respect to frequency, indicative of their fractal character. Simply said: cathode spots, and thus cathodic arcs as a whole, show fractal (self-similar) properties (Anders 2005).

4.2. Plasma deposition

Coming back to the statements that ions are supersonic and often multiply charged: this implies that the plasma flux impinging on a substrate delivers substantially more kinetic and potential energies to a growing film than with other processes such as deposition by evaporation or sputtering. In the case of cathodic arc deposition, the plasma itself condenses and therefore we deal with plasma deposition. The kinetic energy delivered to the growing film can be several 10 eV for each ion, even of order of 100 eV per ion for refractory metals, and typically more than 10 eV of potential energy for each incoming ion (Anders and Yushkov 2002). This is a very large amount of energy deposited locally, sometimes called atomic

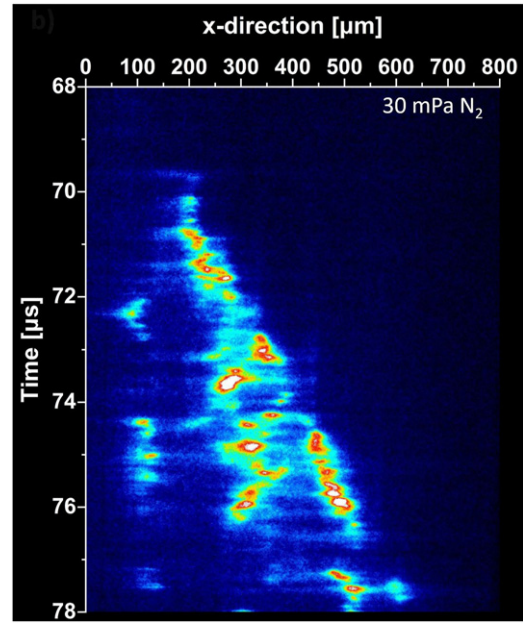


Figure 28. Streak camera image of cathode spots on an aluminum cathode in 30 mPa of nitrogen (light intensity in false colors). The spot appears to move, on average, from left to right in irregular steps. While the on-average direction is affected by the presence of a magnetic field, individual plasma-producing microscopic explosions are random and can occur opposite to the macroscopic apparent motion of the spot. Reprinted from Oh *et al* (2021b), with the permission of AIP Publishing.

scale heating (Anders 2002a). The role of kinetic and potential energies has also been investigated by atomistic simulations of energetic film growth (Kateb *et al* 2021, 2020). The condensable nature of the metal plasma implies that the plasma is not just assisting but the plasma itself is deposited. The sticking coefficient of metal ions is close to unity, however, as studies have shown, the small fraction of non-sticking ions, likely associated with atomic scale heating, represent a flux of neutral atoms leaving the substrate, which has a notable effect on the incoming ion flux due to charge exchange collisions (Anders *et al* 2007). Charge exchange collisions lead to a reduction of the contribution of higher charge states and a corresponding increase of the flux of singly charged ions. The boundary between any plasma and a surface, the sheath, is a space charge layer associated with a voltage drop. The region between a substrate and a cathodic arc plasma also presents a sheath. Even in the absence of an intentional substrate bias, or in the case of a floating substrate, a sheath will form. Even a modest sheath voltage has a substantial effect on the energy of the arriving ions:

$$\mathcal{E}_i = \mathcal{E}_{i0} + QeV_{\text{sheath}}, \quad (23)$$

where \mathcal{E}_{i0} is the energy an ion had already gained in the cathode spot region before acceleration in the substrate's sheath, Q is the charge state number (often 2 or 3 for cathodic arcs), e is the elementary charge, and $V_{\text{sheath}} = V_{\text{plasma}} - V_{\text{surface}}$ is the substrate sheath voltage, i.e. the difference between the plasma potential and the substrate surface potential.

4.3. Substrate bias effects

With intentional (negative) bias, the substrate surface potential is lowered and the sheath voltage thereby increased. For cathodic arcs, bias is generally more effective than with other techniques (such as sputtering) due to the high degree of ionization and the presence of multiply charged ions. At moderate bias of a few 10 V, the deposition process can change its character since the ion energy leads to insertion of the ion under the surface. This therefore results in a subplantation growth process, as opposed to classic film growth processes which assume adding atoms on the surface. Subplantation leads generally to densification of the film, but also to defect formation and enhancement of compressive stress (Bilek and McKenzie 2006). The latter can be excessive as obvious when the deposited film catastrophically break away from the substrate. Indeed, it is generally difficult to grow thick films using a subplantation process. For thin to moderately thick films (say 100 nm or less), subplantation is the preferred method to produce tetrahedral amorphous carbon (ta-C) films, a hydrogen-free form of diamondlike carbon (DLC) films (Abadias *et al* 2018, Pharr *et al* 1996, Uhlmann *et al* 1998). At even higher applied bias, typically of several 100 V, the incoming ions cause substantial sputtering from the growing film. It is possible to increase the bias to a point where more material is removed than deposited: in this case the process becomes ion etching. Combining ion etching and deposition in a two-step process was the underlying idea of ‘arc bond sputtering’ or ABS, i.e., a process starting with high bias etching followed by deposition at lower bias (Münz *et al* 1991). The second (deposition) step was preferably done by sputtering to reduce the ‘macroparticle issue’, a quality reduction caused by the deposition of microscopic cathode droplets or ‘macroparticles’. This issue will require a separate consideration.

4.4. Macroparticles

The high power density at cathode spots implies that there are always regions between the spots and the generally much colder (near room temperature) cathode body. These microscopic regions of melted cathode material are subject to the pressure of the spot plasma: the liquid is pushed from its location and travels from the cathode as microdroplets or macroparticles. The name ‘macroparticle’ has been used in this context for decades (see e.g. Plyutto *et al* (1965)) to express the fact that those particles are orders of magnitude heavier than plasma particles like electrons and ions.

Macroparticles have a velocity of typically a few 10 m s^{-1} to some 100 m s^{-1} , they are much slower than the plasma flow (Schülke and Anders 1999). They cool down during flight and arrive on the substrate in the liquid or solid phase, depending on the material. Low melting point metals form flat ‘pancake’ particles on the surface upon impact (Daalder 1976). Refractory materials, in contrast, are often solidified before impact. They may or may not stick to the substrate: many ‘bounce off’ the surface but some stick and become part of the coating. Macroparticle incorporation into the coatings leads to much enhanced roughness and the deterioration of many other film

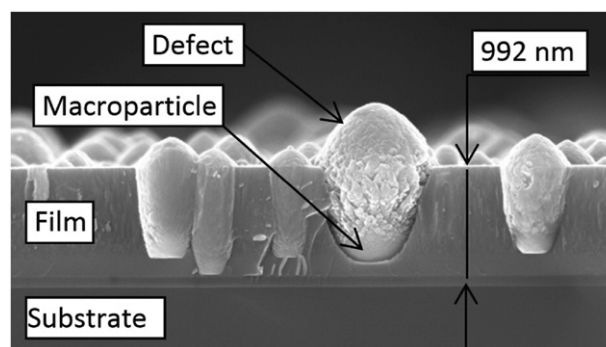


Figure 29. Scanning electron microscope (SEM) image of a cross-section of a film deposited from a $\text{Ti}_{0.3}\text{Al}_{0.7}$ cathode of unfiltered dc arc source at a N_2 pressure of 0.67 Pa. Reprinted from Zhirkov *et al* (2015), Copyright (2015), with permission from Elsevier.

properties. Since the size of a macroparticle can be micrometers in diameter, i.e., larger than the wavelength of visible light, the surface can appear hazy or dull to the eye: upon deposition, the substrate may lose its mirror-like shininess if it was mirror-like before the coating. Macroparticles are the greatest impediment for the even wider use of cathodic arc deposition since the requirements on the quality of coatings is expected to be excellent. Figure 29 illustrates an example when macroparticles are incorporated into a coating thereby greatly affecting (usually in a deleterious way) the properties of the coating (Zhirkov *et al* 2015).

For some applications, the incorporation of macroparticles can be tolerated since other coating qualities are decisive such as hardness, toughness, and of course, low cost. Also, the size of the macroparticles can be reduced by a number of measures: among them is the effect of the reactive gas, the use of ‘spot steering’ and, last but not least, macroparticle filtering. Each of those effects is briefly discussed below.

4.5. Effect of the reactive gas

Similar to magnetron sputtering, the cathode of the arc process reacts with the reactive gas (such as nitrogen or oxygen) when added to the process. The cathode processes are sensitive to the chemical state of the cathode (Jakubka and Jüttner 1981, Oh *et al* 2021b), which is already clear when considering the change in work function (potential barrier) for the electron emission processes. When the cathode is covered with a thin compound layer (‘poisoned cathode’), the ignition of an emission site is often faster (easier), which may be associated with the changed potential structure and/or charge-up in case of an insulating compound. As a result, more cathode spots cover the cathode but each of shorter duration. The current carried by a spot can be reduced from 10 s of amperes to less than 1 ampere. The volume of melted cathode material is much reduced compared to the pure metal case, and, indeed, one finds smaller macroparticles. Moreover, the macroparticles emitted from the cathode also react with the reactive gas, forming a compound, which generally has higher melting point than the cathode metal. When such compound particle arrives at the substrate it is very likely solid and tend (with a high probability) to bounce off and is thus not incorporated in the coating (Karpov 1997).

Cathode poisoning is therefore one of the strategies to reduce macroparticles when depositing compounds.

4.6. Steered arc sources

Another strategy to reduce macroparticles is to make use of the ‘spot steering’ effect on the cathode. Namely, the ignition of cathode spots is affected by the presence of plasma from previous ignitions. When a transverse magnetic field is applied to the cathode (magnetic vector component parallel to the cathode surface), the spot ignition probability is not isotropic but there is a preferred direction due to the magnetic field effect on the plasma of previous spots (Robson and von Engel 1956). This can be used to ‘steer’ the arc in a preferred direction. The path can be closed—similar to an erosion ‘racetrack’ that is formed in the target surface of a magnetron sputtering discharge. The ‘speed’ of spot motion can be enhanced when the magnetic field is strong. As a side effect, the spot emission time is reduced, leading to less cathode melting and less macroparticles. Of course, the steering effect can be combined with the strategy of cathode poisoning. However, even in the best cases, the coatings still contain macroparticles.

4.7. Macroparticle filtering

For applications, where macroparticles are highly detrimental, like in optical coatings applications, the previous measures are not sufficient, and one can apply a filtering process that separates plasma (ions, electrons) from macroparticles based on the fact that macroparticles are so much heavier than plasma particles. The plasma is guided to a substrate that is not in line-of-sight with the cathode (Aksenov *et al* 1978). Guiding the plasma is generally accomplished by using a curved magnetic field that connects the region of plasma generation (cathode surface where spots burn) with the substrate where the coatings should be deposited. Various geometries of macroparticle filters have been invented and tested (Anders 1999). One such macroparticle filter is shown in figure 30. The filters are based on the general principle that electrons are easily magnetized and, on average, effectively follow magnetic field lines. The motion of ions, in turn, is affected by the motion of electrons: the plasma tends to stay quasi-neutral due to strong electric fields that immediately arise when electrons and ions separate. Plasma transport in macroparticle filters is thus facilitated by a combined magnetic and electric field mechanism. While macroparticle filters are effective, there is also a substantial plasma loss in the transport, which implies a loss of deposition rate (Aksenov *et al* 2003). The largest advantage of cathodic arc plasma deposition, its high deposition rate, is therefore diminished. Filtered arc deposition has therefore only be applied in few applications. The vast majority of industrial cathodic arc deposition systems limit themselves to utilizing the cathode poisoning and spot steering approaches.

4.8. Using the advantages of cathodic arc plasma for PVD

After elaborating at length about the macroparticle issue and macroparticle mitigation strategies such as macroparticle filtering, we ought to also address why cathodic arc deposition is a widely used PVD technique. Most importantly, the cathodic

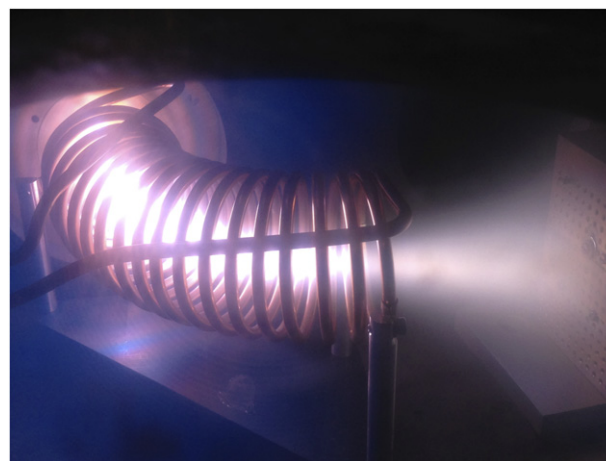


Figure 30. Example of an open-coil 90-degree filter, here to filter plasma from an aluminum-doped zinc cathode in the presence of oxygen to deposit high-quality AZO (aluminum-doped zinc oxide). Reprinted from Anders, (2014), Copyright (2014), with permission from Elsevier.

arc discharge is a prolific, efficient and economical generator of plasma of the cathode material. As a low voltage, high current process, arcs produce a high flux of condensable and ionized material and deliver it onto a substrate with high energy efficiency. High deposition rate, low cost as well as being capable of delivering desirable film properties made cathodic arc deposition a preferred choice for some coatings applications over the last decades. The very high degree of ionization of the flux allows producers of coatings to effectively use bias, thereby controlling the energy of deposited particles, which in turn affects the microstructure and related properties (see discussion in section 1 and around figure 3). Arc deposition is therefore both an economical and flexible approach to produce coatings in a wide range of composition and microstructure. This is especially established for hard, tough, and oxidation-resistant tool coatings like TiAlN (see e.g. Hans *et al* (2019) and/or Schultrich (2022)) and diamondlike carbon coatings (Vetter 2014).

5. Conclusion

The different PVD techniques are discussed and shown that they provide depositing fluxes that vary in absolute value, in ionization degree, and in species composition and energy. This includes deposition by thermal evaporation, electron beam evaporation, magnetron sputtering, ion beam sputtering, laser ablation, and cathodic arc deposition (while this list contains the most important methods, no claim of completeness is made since a variety of other techniques exist, including hybrid techniques of the above). The variations in the deposition flux have influence on the film microstructure and morphology and therefore on the film structural properties, composition, mass density, optical properties, the stress in the film, electrical resistivity and surface roughness. In fact, PVD stands for a collection of versatile deposition techniques, that have a variety of applications. Most importantly, these techniques are the basis for many approaches applied in material science, where

the synthesis of a material with superior quality or of films from a metastable compound can only be realised by PVD.


Acknowledgments

This work was partially supported by the Icelandic Research Fund Grant No. 196141, the German Science Foundation under the umbrella of the SFB TR 87, and the Leibniz Association via the Collaborative Excellence Project K128/2018.

Data availability statement

The data that support the findings of this study are available upon reasonable request from the authors.

ORCID iDs

Jon Tomas Gudmundsson  <https://orcid.org/0000-0002-8153-3209>

André Anders  <https://orcid.org/0000-0002-5313-6505>

Achim von Keudell  <https://orcid.org/0000-0003-3887-9359>

References

- Abadias G *et al* 2018 *J. Vac. Sci. Technol. A* **36** 020801
- Affinito J and Parsons R R 1984 *J. Vac. Sci. Technol. A* **2** 1275–84
- Aisenberg S and Chabot R W 1973 *J. Vac. Sci. Technol. A* **10** 104–7
- Aksenov I I, Belous V A, Padalka V G and Khoroshikh V M 1978 *Instrum. Exp. Tech.* **21** 1416–8
- Aksenov I I, Strel'nitskij V E, Vasilyev V V and Zaleskij D Y 2003 *Surf. Coat. Technol.* **163–164** 118–27
- Amin N and Rahman K S 2017 Close-spaced sublimation (CSS): a low-cost, high-yield deposition system for cadmium telluride (CdTe) thin film solar cells *Modern Technologies for Creating the Thin-Film Systems and Coatings* ed N Nikitenkov (London: InTechOpen) ch 18 pp 361–79
- Anders A 1999 *Surf. Coat. Technol.* **120–121** 319–30
- Anders A 2002a *Appl. Phys. Lett.* **80** 1100–2
- Anders A 2003 *IEEE Trans. Plasma Sci.* **31** 1052–9
- Anders A 2005 *IEEE Trans. Plasma Sci.* **33** 1456–64
- Anders A 2006 *Thin Solid Films* **502** 22–8
- Anders A 2008 *Cathodic Arcs: From Fractal Spots to Energetic Condensation (Springer Series on Atomic, Optical, and Plasma Physics vol 50)* (New York: Springer)
- Anders A 2010 *Thin Solid Films* **518** 4087–90
- Anders A 2012 *Appl. Phys. Lett.* **100** 224104
- Anders A 2017 *J. Appl. Phys.* **121** 171101
- Anders A, Anders S, Jüttner B, Botticher W, Luck H and Schroder G 1992 *IEEE Trans. Plasma Sci.* **20** 466–72
- Anders A, Anders S, Jüttner B and Luck H 1996 *IEEE Trans. Plasma Sci.* **24** 69–70
- Anders A, Fukuda K and Yushkov G Y 2005 *J. Phys. D: Appl. Phys.* **38** 1021–8
- Anders A, Oks E M and Yushkov G Y 2007 *J. Appl. Phys.* **102** 043303
- Anders A 2002b Cohesive energy rule for vacuum arcs *Emerging Applications of Vacuum-Arc-Produced Plasma, Ion and Electron Beams (NATO Science Series II: Mathematics, Physics and Chemistry vol 88)* ed E Oks and I Brown (Dordrecht: Kluwer) pp 1–14
- Anders A and Yang Y 2017 *Appl. Phys. Lett.* **111** 064103
- Anders A and Yushkov G Y 2002 *J. Appl. Phys.* **91** 4824–32
- Anderson G S, Mayer W N and Wehner G K 1962 *J. Appl. Phys.* **33** 2991–2
- Arthur J R 2002 *Surf. Sci.* **500** 189–217
- Barnes M S, Forster J C and Keller J H 1993 Apparatus for depositing material into high aspect ratio holes *US Patent* 5,178,739 (New York: International Business Machines Corporation, Armonk)
- Bean J C 1993 Techniques for the growth of crystalline films by molecular beam deposition *Multicomponent and Multilayered Thin Films for Advanced Microtechnologies: Techniques, Fundamentals and Devices (NATO ASI Series E: Applied Sciences vol 234)* ed O Auciello and J Engemann (Dordrecht: Kluwer) pp 87–107
- Berry L A and Gorbalkin S M 1995 *J. Vac. Sci. Technol. A* **13** 343–8
- Biersack J P and Haggmark L G 1980 *Nucl. Instrum. Methods* **174** 257–69
- Bilek M M M and McKenzie D R 2006 *Surf. Coat. Technol.* **200** 4345–54
- Biskup B, Maszl C, Breilmann W, Held J, Böke M, Benedikt J and von Keudell A 2018 *J. Phys. D: Appl. Phys.* **51** 115201
- Blondeel A, Delrue H, Matthews S, Van Holsbeke J and De Bosscher W 2006 Advantages of using rotating cylindrical ITO targets for large area coating applications *Proc. 49th Annual Technical Conf. Proc.* (Washington DC 22–27 April 2006) (Albuquerque, New Mexico: Society of Vacuum Coaters) pp 187–91
- Bobzin K, Brögelmann T, Kruppe N C, Engels M, von Keudell A, Hecimovic A, Ludwig A, Grochla D and Banko L 2017 *J. Appl. Phys.* **122** 015302
- Boeuf J P and Takahashi M 2020a *Phys. Plasmas* **27** 083520
- Boeuf J-P 2014 *Front. Phys.* **2** 74
- Boeuf J-P and Takahashi M 2020b *Phys. Rev. Lett.* **124** 185005
- Boxman R L, Sanders D M and Martin P J (ed) 1995 *Handbook of Vacuum Arc Science and Technology: Fundamentals and Applications* (Park Ridge, New Jersey: Noyes Publications)
- Bradley J W, Thompson S and Gonzalvo Y A 2001 *Plasma Sources Sci. Technol.* **10** 490–501
- Brenning N, Butler A, Hajihoseini H, Rudolph M, Raadu M A, Gudmundsson J T, Minea T and Lundin D 2020 *J. Vac. Sci. Technol. A* **38** 033008
- Brenning N, Gudmundsson J T, Lundin D, Minea T, Raadu M A and Helmersson U 2016 *Plasma Sources Sci. Technol.* **25** 065024
- Brenning N, Hajihoseini H, Rudolph M, Raadu M A, Gudmundsson J T, Minea T M and Lundin D 2021 *Plasma Sources Sci. Technol.* **30** 015015
- Brenning N, Lundin D, Minea T, Costin C and Vitelaru C 2013 *J. Phys. D: Appl. Phys.* **46** 084005
- Brown I G 1994 *Rev. Sci. Instrum.* **65** 3061–81
- Brückner J, Teschner G, Milde F and Krause J 2005 Advanced rotatable magnetron module designed for large area glass coaters *Proc. 48th Society of Vacuum Coaters Annual Technical Conf.* (Denver, Colorado 23–28 April 2005) (Albuquerque, New Mexico: Society of Vacuum Coaters) pp 265–9
- Bultinck E and Bogaerts A 2009 *New J. Phys.* **11** 103010
- Bundesmann C and Neumann H 2018 *J. Appl. Phys.* **124** 231102
- Byon E and Anders A 2003 *J. Appl. Phys.* **93** 1899–906
- Chabert P, Tsankov T V and Czarnetzki U 2021 *Plasma Sources Sci. Technol.* **30** 024001
- Chapin J S 1974 *Res. Dev.* **25**(1) 37–40

- Chapin J S 1979 Sputtering process and apparatus *US Patent* 4166018A (Montvale, New Jersey, United States of America: Aircro, Inc.)
- Cheung J T and Sankur H 1988 *Crit. Rev. Solid State Mater. Sci.* **15** 63–109
- Cheung J and Horwitz J 1992 *MRS Bull.* **17** 30–6
- Chistyakov R and Abraham B 2009 Advanced pulsed DC technology for material processing applications: II. Plasma generator for arbitrary voltage pulse shape *SVC Bulletin (Summer)* pp 32–6
- Cho A Y 1971 *J. Vac. Sci. Technol.* **8** S31–8
- Cho A Y 1995 *MRS Bull.* **20** 21–8
- Christie D J 2005 *J. Vac. Sci. Technol. A* **23** 330–5
- Daalder J E 1976 *J. Phys. D: Appl. Phys.* **9** 2379–95
- Daalder J E 1979 *J. Phys. D: Appl. Phys.* **12** 1769–79
- Davids P D and Maissel L I 1966 *J. Appl. Phys.* **37** 574–9
- Davis W D and Miller H C 1969 *J. Appl. Phys.* **40** 2212–21
- Dijkkamp D, Venkatesan T, Wu X D, Shaheen S A, Jisrawi N, Min-Lee Y H, McLean W L and Croft M 1987 *Appl. Phys. Lett.* **51** 619–21
- Eason R 2007 *Pulsed Laser Deposition of Thin Films: Applications-Led Growth of Functional Materials* (New York: Wiley)
- Ebeling W and Kilimann K 1989 *Z. Naturforsch. A* **44** 519–23
- Eckstein W 2007 Sputtering yields *Sputtering by Particle Bombardment: Experiments and Computer Calculations from Threshold to MeV Energies (Topics in Applied Physics vol 110)* ed R Behrisch and W Eckstein (Berlin: Springer) pp 33–187
- Ehiasarian A P, Hecimovic A, de los Arcos T, New R, Schulz-von der Gathen V, Böke M and Winter J 2012 *Appl. Phys. Lett.* **100** 114101
- Este G and Westwood W D 1988 *J. Vac. Sci. Technol. A* **6** 1845–8
- Ferreira F, Oliveira J C and Cavaleiro A 2016 *Surf. Coat. Technol.* **291** 365–75
- Ferreira F, Serra R, Oliveira J C and Cavaleiro A 2014 *Surf. Coat. Technol.* **258** 249–56
- Franz R, Clavero C, Kolbeck J and Anders A 2016 *Plasma Sources Sci. Technol.* **25** 015022
- Fruth H F 1932 *Physics* **2** 280–6
- Fujioka H 2015 Pulsed laser deposition (PLD) *Thin Films and Epitaxy: Basic Techniques (Part A of Handbook of Crystal Growth vol 3)* 2nd edn ed T Kuech (Amsterdam, The Netherlands: Elsevier) ch 4 pp 365–97
- Gall D 2005 Vapor transport processing: mechanisms *Encyclopedia of Condensed Matter Physics* ed F Bassani, G L Liedl and P Wyder (New York: Academic) pp 291–6
- Gibson U J 1987 Ion-beam processing of optical thin films *Advances in Research and Development (Physics of Thin Films vol 13)* ed M H Francombe and J L Vossen (New York: Academic) pp 109–50
- Gill W D and Kay E 1965 *Rev. Sci. Instrum.* **36** 277–82
- Gnaser H 2007 Energy and angular distributions of sputtered species *Sputtering by Particle Bombardment: Experiments and Computer Calculations from Threshold to MeV Energies (Topics in Applied Physics vol 110)* ed R Behrisch and W Eckstein (Berlin: Springer) ch 5 pp 231–328
- Goldberg O, Goldenberg E, Zhitomirsky V N, Cohen S R and Boxman R L 2012 *Surf. Coat. Technol.* **206** 4417–24
- Gorbatkin S M, Poker D B, Rhoades R L, Doughty C, Berry L A and Rossnagel S M 1996 *J. Vac. Sci. Technol. B* **14** 1853–9
- Grafer E B 2017 Electron beam evaporation *Handbook of Thin Film Process Technology* ed D A Glocker and S I Shah (Boca Raton, Florida: CRC Press) p A1.2
- Greczynski G, Petrov I, Greene J E and Hultman L 2019 *J. Vac. Sci. Technol. A* **37** 060801
- Green K M, Hayden D B, Juliano D R and Ruzic D N 1997 *Rev. Sci. Instrum.* **68** 4555–60
- Greene J E and Barnett S A 1982 *J. Vac. Sci. Technol.* **21** 285–302
- Gudmundsson J T 2008 *J. Phys.: Conf. Ser.* **100** 082002
- Gudmundsson J T 2020 *Plasma Sources Sci. Technol.* **29** 113001
- Gudmundsson J T, Brenning N, Lundin D and Helmersson U 2012 *J. Vac. Sci. Technol. A* **30** 030801
- Gudmundsson J T and Hecimovic A 2017 *Plasma Sources Sci. Technol.* **26** 123001
- Gudmundsson J T and Lundin D 2020 Introduction to magnetron sputtering *High Power Impulse Magnetron Sputtering: Fundamentals, Technologies, Challenges and Applications* ed D Lundin, T Minea and J T Gudmundsson (Amsterdam, The Netherlands: Elsevier) pp 1–48
- Hajihoseini H, Čada M, Hubička Z, Ünalı S, Raadu M A, Brenning N, Gudmundsson J T and Lundin D 2019 *Plasma* **2** 201–21
- Hajihoseini H and Gudmundsson J T 2017 *J. Phys. D: Appl. Phys.* **50** 505302
- Hála M 2011 Characterization of high power impulse magnetron sputtering discharges *PhD Thesis* École Polytechnique de Montréal, Montréal, Canada
- Hála M, Čapek J, Zabeida O, Klemberg-Sapieha J E and Martinu L 2012 *Surf. Coat. Technol.* **206** 4186–93
- Hans M *et al* 2019 *Coatings* **9** 24
- Harper J M E 1990 Particle bombardment effects in thin film deposition *Plasma-Surface Interactions and Processing of Materials (NATO ASI Series E: Applied Sciences vol 176)* ed O Auciello, A Gras-Martı, J A Valles-Abarca and D L Flamm (Dordrecht: Kluwer) pp 251–80
- Harper J M E 1978 Ion beam deposition *Thin Film Processes* ed J L Vossen and J J Cuomo (New York: Academic) pp 175–206
- Heister U, Krempel-Hesse J, Szczyrbowski J, Teschner G, Bruch J and Bräuer G 2000 *Vacuum* **59** 424–30
- Held J, Hecimovic A, von Keudell A and Schulz-von der Gathen V 2018 *Plasma Sources Sci. Technol.* **27** 105012
- Held J, Maaß P A, Schulz-von der Gathen V and von Keudell A 2020 *Plasma Sources Sci. Technol.* **29** 025006
- Helmersson U, Lattemann M, Bohlmark J, Ehiasarian A P and Gudmundsson J T 2006 *Thin Solid Films* **513** 1–24
- Herman M A and Sitter H 1996 *Molecular Beam Epitaxy: Fundamentals and Current Status (Springer Series in Materials Science vol 7)* 2nd edn (Berlin: Springer)
- Hofer W O 1991 Angular, energy, and mass distribution of sputtered particles *Sputtering by Particle Bombardment III: Characteristics of Sputtered Particles, Technical Applications (Topics in Applied Physics vol 64)* ed R Behrisch and K Wittmaack (Berlin: Springer) pp 15–90
- Holber W M 2000 Ionization by microwave electron cyclotron resonance plasma *Ionized Physical Vapor Deposition (Thin Films vol 27)* ed J A Hopwood (San Diego, California: Academic) pp 67–94
- Holber W M, Logan J S, Grabarz H J, Yeh J T C, Caughman J B O, Sugerman A and Turene F E 1993 *J. Vac. Sci. Technol. A* **11** 2903–10
- Hopwood J A 2000 The role of ionized physical vapor deposition in integrated circuit fabrication *Ionized Physical Vapor Deposition (Thin Films vol 27)* ed J A Hopwood (San Diego, California: Academic) pp 1–7
- Hopwood J 1992 *Plasma Sources Sci. Technol.* **1** 109–16
- Hopwood J 1998 *Phys. Plasmas* **5** 1624–31
- Hopwood J, Guarnieri C R, Whitehair S J and Cuomo J J 1993 *J. Vac. Sci. Technol. A* **11** 152–6
- Hubička Z, Gudmundsson J T, Larsson P and Lundin D 2020 Hardware and power management for high power impulse magnetron sputtering *High Power Impulse Magnetron Sputtering: Fundamentals, Technologies, Challenges and Applications* ed D Lundin, T Minea and J T Gudmundsson (Amsterdam, The Netherlands: Elsevier) pp 49–80
- Huo C, Lundin D, Gudmundsson J T, Raadu M A, Bradley J W and Brenning N 2017 *J. Phys. D: Appl. Phys.* **50** 354003

- Huo C, Lundin D, Raadu M A, Anders A, Gudmundsson J T and Brenning N 2013 *Plasma Sources Sci. Technol.* **22** 045005
- Hussein A E, Diwakar P K, Harilal S S and Hassanein A 2013 *J. Appl. Phys.* **113** 143305
- Jakubka K and Jüttner B 1981 *J. Nucl. Mater.* **102** 259–66
- Janes G S and Lowder R S 1966 *Phys. Fluids* **9** 1115–23
- Jüttner B 2001 *J. Phys. D: Appl. Phys.* **34** R103–23
- Jüttner B, Pursch H and Anders S 1984 *J. Phys. D: Appl. Phys.* **17** L111–4
- Kadlec S, Musil J and Vyskočil H 1986 *J. Phys. D: Appl. Phys.* **19** L187–90
- Karpov D A 1997 *Surf. Coat. Technol.* **96** 22–33
- Kateb M, Gudmundsson J T, Brault P, Manolescu A and Ingvarsson S 2021 *Surf. Coat. Technol.* **426** 127726
- Kateb M, Gudmundsson J T and Ingvarsson S 2020 *J. Vac. Sci. Technol. A* **38** 043006
- Kateb M, Hajihoseini H, Gudmundsson J T and Ingvarsson S 2019 *J. Vac. Sci. Technol. A* **37** 031306
- Kaufman H R and Robinson R S 1989 *Vacuum* **39** 1175–80
- Kawamura E, Vahedi V, Lieberman M A and Birdsall C K 1999 *Plasma Sources Sci. Technol.* **8** R45–64
- Kay E 1963 *J. Appl. Phys.* **34** 760–8
- Kay E 1962 Impact evaporation (sputtering) and thin film growth in a glow discharge *Advances of Electronics and Electron Physics* vol 17 ed L L Marton (New York: Academic) pp 245–322
- Kelly P J and Arnell R D 1998 *Surf. Coat. Technol.* **108–109** 317–22
- Kelly P J and Arnell R D 2000 *Vacuum* **56** 159–72
- Kelly P 2011 *Mater. Technol.* **26** 1–2
- Keraudy J, Viloin R P B, Raadu M A, Brenning N, Lundin D and Helmersson U 2019 *Surf. Coat. Technol.* **359** 433–7
- Klawuhn E, D' Couto G C, Ashtiani K A, Rymer P, Biberger M A and Levy K B 2000 *J. Vac. Sci. Technol. A* **18** 1546–9
- Knodle W S and Chow R 2002 Molecular beam epitaxy: equipment and practice *Deposition Processes and Techniques: Principles, Methods, Equipment and Applications* 2nd edn ed K Seshan (Norwich, New York: Noyes Publications) pp 381–461
- Kolev I, Bogaerts A and Gijbels R 2005 *Phys. Rev. E* **72** 056402
- Kouznetsov V, Macák K, Schneider J M, Helmersson U and Petrov I 1999 *Surf. Coat. Technol.* **122** 290–3
- Kozyrev A V, Sochugov N S, Oskomov K V, Zakharov A N and Odivanova A N 2011 *Plasma Phys. Rep.* **37** 621–7
- Krüger D, Köhn K, Gallian S and Brinkmann R P 2018 *Phys. Plasmas* **25** 061207
- Kubart T, Gudmundsson J T and Lundin D 2020 Reactive high power impulse magnetron sputtering *High Power Impulse Magnetron Sputtering: Fundamentals, Technologies, Challenges and Applications* ed D Lundin, T Minea and J T Gudmundsson (Amsterdam, The Netherlands: Elsevier) pp 223–63
- Lafferty J M 1980 *Vacuum Arcs: Theory and Application* (New York: Wiley)
- Lai K F 2000 Ionized hollow cathode magnetron sputtering *Ionized Physical Vapor Deposition (Thin Films vol 27)* ed J A Hopwood (San Diego, California: Academic) pp 95–139
- Layes V 2021 Fundamental surface processes in HiPIMS plasmas: physics and chemistry at the plasma magnetron target interface *PhD Thesis Ruhr-Universität Bochum, Germany*
- Lieberman M A and Lichtenberg A J 2005 *Principles of Plasma Discharges and Materials Processing* 2nd edn (New York: Wiley)
- Liebig B, Braithwaite N S J, Kelly P J, Chistyakov R, Abraham B and Bradley J W 2011 *Surf. Coat. Technol.* **205** S312–6
- Lin J, Sproul W D, Moore J J, Wu Z, Lee S, Chistyakov R and Abraham B 2011 *JOM* **63** 48–58
- Logan J S 1990 RF sputter etching and deposition *Handbook of Plasma Processing Technology: Fundamentals, Etching, Deposition, and Surface Engineering* ed S M Rosnagel, W D Westwood and J J Cuomo (Park Ridge, NJ: Noyes Publications) pp 140–59
- Lou B-S, Chen W-T, Diyatmika W, Lu J-H, Chang C-T, Chen P-W and Lee J-W 2021 *Surf. Coat. Technol.* **421** 127430
- Lundin D, Vitellari C, de Pouques L, Brenning N and Minea T 2013 *J. Phys. D: Appl. Phys.* **46** 175201
- Mahan J E 2000 *Physical Vapor Deposition of Thin Films* (New York: Wiley)
- Mahieu S, Van Aeken K and Depla D 2008 Transport of sputtered particles through the gas phase *Reactive Sputter Deposition* ed D Depla and S Mahieu (*Springer Series in Materials Science* vol 109) ch 6 (Berlin: Springer) pp 199–227
- Martin L W, Chu Y-H and Ramesh R 2010 *Mater. Sci. Eng. R* **68** 89–133
- Martin P 1990 *IEEE Trans. Plasma Sci.* **18** 855–68
- Matthews A and Teer D G 1980 *Thin Solid Films* **72** 541–9
- Mattox D M 1998 *Handbook of Physical Vapor Deposition (PVD) Processing: Film Formation, Adhesion, Surface Preparation and Contamination Control* (Westwood, New Jersey: Noyes Publications)
- McKelvey H E 1982 Magnetron cathode sputtering apparatus *US Patent 4356073* (Detroit, Michigan: Shatterproof Glass Corporation)
- McLennan J C, Ainslie D S and Fuller D S 1919 *Proc. R. Soc. A* **95** 316–32
- McNeil J R, McNally J J and Reader P D 2002 Ion beam deposition *Handbook of Thin-Film Deposition Processes and Techniques: Principles, Methods, Equipment and Applications* 2nd edn ed K Seshan (Norwich, New York: Noyes Publications) pp 463–99
- Mesyats G A 1998 *Explosive Electron Emission* (Ekaterinburg: URO Press)
- Mesyats G A and Proskurovsky D I 1989 *Pulsed Electrical Discharge in Vacuum (Springer Series on Atomic, Optical, and Plasma Physics vol 5)* (Berlin: Springer)
- Metz G E 2012 Characterization of a plasma reactor device for photo-voltaic applications *Master's Thesis* Colorado State University, Fort Collins, Colorado
- Mishra A, Kelly P J and Bradley J W 2010 *Plasma Sources Sci. Technol.* **19** 045014
- Mitchell K, Fahrenbruch A L and Bube R H 1975 *J. Vac. Sci. Technol.* **12** 909–11
- Möller W and Eckstein W 1984 *Nucl. Instrum. Methods Phys. Res. B* **2** 814–8
- Möller W, Eckstein W and Biersack J P 1988 *Comput. Phys. Commun.* **51** 355–68
- Monaghan D P, Teer D G, Laing K C, Efeoglu I and Arnell R D 1993 *Surf. Coat. Technol.* **59** 21–5
- Morley J R and Smith H R 1972 *J. Vac. Sci. Technol.* **9** 1377–8
- Münz W-D, Hauzer F J M, Schulze D and Buil B 1991 *Surf. Coat. Technol.* **49** 161–7
- Murayama Y 1974 *Japan. J. Appl. Phys.* **13** 459–62
- Musil J, Kadlec S and Münz W D 1991 *J. Vac. Sci. Technol. A* **9** 1171–7
- Nakano T, Hirukawa N, Saeki S and Baba S 2013 *Vacuum* **87** 109–13
- Nakano T, Murata C and Baba S 2010 *Vacuum* **84** 1368–71
- Nakano T, Saitou Y and Oya K 2017 *Surf. Coat. Technol.* **326** 436–42
- Nakano T, Umahashi T and Baba S 2014 *Japan. J. Appl. Phys.* **53** 028001
- Oh K, Kalanov D and Anders A 2021a *Plasma Sources Sci. Technol.* **30** 095005
- Oh K, Kalanov D, Birtel P and Anders A 2021b *J. Appl. Phys.* **130** 183304
- Ojeda-G-P A, Döbeli M and Lippert T 2018 *Adv. Mater. Interfaces* **5** 1701062
- Okamoto A and Serikawa T 1986 *Thin Solid Films* **137** 143–51

- Ono T, Takahashi C and Matsuo S 1984 *Japan. J. Appl. Phys.* **23** L534–6
- Panjan M and Anders A 2017 *J. Appl. Phys.* **121** 063302
- Panjan M, Franz R and Anders A 2014 *Plasma Sources Sci. Technol.* **23** 025007
- Parker E H C (ed) 1985 *The Technology and Physics of Molecular Beam Epitaxy* (New York: Plenum)
- Petrea M-A and Stamate E 2021 *Plasma Sources Sci. Technol.* **30** 045002
- Petrov I, Barna P B, Hultman L and Greene J E 2003 *J. Vac. Sci. Technol. A* **21** S117–28
- Pharr G M *et al* 1996 *Appl. Phys. Lett.* **68** 779–81
- Plyutto A A, Ryzhkov V N and Kapin A T 1965 *Sov. Phys. - JETP* **20** 328–37 http://jetp.ras.ru/cgi-bin/dn/e_020_02_0328.pdf
- Poolcharuansin P, Liebig B and Bradley J W 2012 *Plasma Sources Sci. Technol.* **21** 015001
- Preissing S 2016 Spectroscopic investigation of an extensive magnetron plasma *Master's Thesis* Ruhr Universität Bochum, Germany
- Priestley J 1775 *The History and Present State of Electricity* 3rd edn (London, England)
- Ptak A J 2015 Principles of molecular beam epitaxy *Thin Films and Epitaxy: Basic Techniques (Part A of Handbook of Crystal Growth* vol 3) 2nd edn, ed T Kuech (Amsterdam: Elsevier) ch 4 pp 161–92
- Rahman K S, Harif M N, Rosly H N, Kamaruzzaman M I B, Akhtaruzzaman M, Alghoul M, Misran H and Amin N 2019 *Results Phys.* **14** 102371
- Rauch A and Anders A 2013 *Vacuum* **89** 53–6
- Rauschenbach B 2002 *Vacuum* **69** 3–10
- Ready J 1971 *Effects of High-Power Laser Radiation* (New York: Academic)
- Robson A E and von Engel A 1956 *Phys. Rev.* **104** 15–6
- Rohde S L 1994 Unbalanced magnetron sputtering *Plasma Sources for Thin Film Deposition and Etching (Physics of Thin Films* vol 18) ed M H Francombe and J L Vossen (New York: Academic) pp 235–88
- Rossnagel S M 1999 *IBM J. Res. Dev.* **43** 163–79
- Rossnagel S M 2003 *J. Vac. Sci. Technol. A* **21** S74–87
- Rossnagel S M and Cuomo J J 1988 *MRS Bull.* **13** 40–5
- Rossnagel S M and Hopwood J 1993 *Appl. Phys. Lett.* **63** 3285–7
- Rossnagel S M and Hopwood J 1994 *J. Vac. Sci. Technol. B* **12** 449–53
- Rossnagel S 2000 Ionization by radio frequency inductively coupled plasma *Ionized Physical Vapor Deposition (Thin Films* vol 27) ed J A Hopwood (New York: Academic) pp 37–66
- Rudolph M, Brenning N, Hajihoseini H, Raadu M A, Minea T M, Anders A, Gudmundsson J T and Lundin D 2022 *J. Phys. D: Appl. Phys.* **55** 015202
- Rudolph M, Brenning N, Raadu M A, Hajihoseini H, Gudmundsson J T, Anders A and Lundin D 2020 *Plasma Sources Sci. Technol.* **29** 05LT01
- Samuelsson M, Lundin D, Jensen J, Raadu M A, Gudmundsson J T and Helmersson U 2010 *Surf. Coat. Technol.* **205** 591–6
- Sarakinos K, Alami J and Konstantinidis S 2010 *Surf. Coat. Technol.* **204** 1661–84
- Sarakinos K, Alami J and Wuttig M 2007 *J. Phys. D: Appl. Phys.* **40** 2108–14
- Scherer M, Schmitt J, Latz R and Schanz M 1992 *J. Vac. Sci. Technol. A* **10** 1772–6
- Schiller S, Goedicke K, Reschke J, Kirchhoff V, Schneider S and Milde F 1993 *Surf. Coat. Technol.* **61** 331–7
- Schiller S, Heisig U, Korndörfer C, Beister G, Reschke J, Steinfelder K and Strümpfel J 1987 *Surf. Coat. Technol.* **33** 405–23
- Schiller S, Heisig U, Steinfelder K, Strümpfel J, Voigt R, Fendler R and Teschner G 1982 *Thin Solid Films* **96** 235–40
- Schülke T and Anders A 1999 *Plasma Sources Sci. Technol.* **8** 567–71
- Schultrich B 2022 *Coatings* **12** 109
- Sellers J 1998 *Surf. Coat. Technol.* **98** 1245–50
- Shen J, Gai Z and Kirschner J 2004 *Surf. Sci. Rep.* **52** 163–218
- Shimizu T, Zanaška M, Villoan R P, Brenning N, Helmersson U and Lundin D 2021 *Plasma Sources Sci. Technol.* **30** 045006
- Sigmund P 1969 *Phys. Rev.* **184** 383–416
- Smeets R P P and Schulpen F J H 1988 *J. Phys. D: Appl. Phys.* **21** 301–10
- Spitzer L 1956 *Physics of Fully Ionized Gases* (New York: Interscience)
- Sproul W D 1998 *Vacuum* **51** 641–6
- Sproul W D, Christie D J and Carter D C 2005 *Thin Solid Films* **491** 1–17
- Sproul W D, Rudnik P J, Graham M E and Rohde S L 1990 *Surf. Coat. Technol.* **43–44** 270–8
- Sproul W D and Tomashek J R 1984 Rapid rate reactive sputtering of a group IVB metal *US Patent* 4,428,811 (Chicago, Illinois, United States of America: Borg-Warner Corporation)
- Stamate E 2020 *Surf. Coat. Technol.* **402** 126306
- Stelmack L A, Thurman C T and Thompson G R 1989 *Nucl. Instrum. Methods Phys. Res. B* **37–38** 787–93
- Stepanova M and Dew S K 2004 *Nucl. Instrum. Methods Phys. Res. B* **215** 357–65
- Stolz C J and Génin F Y 2003 Laser resistant coatings *Optical Interference Coatings (Springer Series in Optical Sciences* vol 88) ed N Kaiser and H K Pulker (Berlin: Springer) pp 309–33
- Strijkmans K, Schelfhout R and Depla D 2018 *J. Appl. Phys.* **124** 241101
- Swanson D E, Geisthardt R M, McGoffin J T, Williams J D and Sites J R 2013 *IEEE J. Photovoltaics* **3** 838–42
- Swanson D E, Kephart J M, Kobayakov P S, Walters K, Cameron K C, Barth K L, Sampath W S, Drayton J and Sites J R 2016 *J. Vac. Sci. Technol. A* **34** 021202
- Swanson D E, Lutze R M, Sampath W S and Williams J D 2011 Plasma cleaning of TCO surfaces prior to CdS/CdTe deposition *38th IEEE Photovoltaic Specialists Conf.* (Austin, Texas 3–8 June 2012) (IEEE) pp 859–63
- Takahashi C, Kiuchi M, Ono T and Matsuo S 1988 *J. Vac. Sci. Technol. A* **6** 2348–52
- Tanberg R 1930 *Phys. Rev.* **35** 1080–9
- Teer D G 1976 *J. Phys. D: Appl. Phys.* **9** L187–9
- Thompson M W 1968 *Phil. Mag.* **18** 377–414
- Thompson M W 1981 *Phys. Rep.* **69** 335–71
- Thornton J A 1988 Physical vapor deposition *Semiconductor Materials and Process Technology Handbook for Very Ultra Large Scale Integration (VLSI) and Ultra Large Scale Integration (ULSI)* ed G F McGuire (Norwich, New York: Noyes Publications) pp 329–454
- Thornton J A and Penfold A S 1978 Cylindrical magnetron sputtering *Thin Film Processes* vol 4 ed J L Vossen and W Kern (New York: Academic) pp 75–113
- Tsikata S and Minea T 2015 *Phys. Rev. Lett.* **114** 185001
- Uhlmann S, Frauenheim T and Lifshitz Y 1998 *Phys. Rev. Lett.* **81** 641–4
- Vetter J 2014 *Surf. Coat. Technol.* **257** 213–40
- Vetushka A, Brown R, Azzopardi A, Bellido-Gonzalez V, Li H and Papa F 2015 Full face erosion planar cathodes as a low cost cylindrical rotatable R & D tool *Proc. 58th Society of Vacuum Coaters Annual Technical Conf.* (Santa Clara, California 25–30 April 2015) (Albuquerque, New Mexico: Society of Vacuum Coaters) pp 566–70
- Vossen J L 1971 *J. Vac. Sci. Technol.* **8** S12–30
- Vossen J L and Cuomo J J 1978 Glow discharge sputter deposition *Thin Film Processes* vol 4 ed J L Vossen and W Kern (New York: Academic) pp 11–73
- Vossen J L and O'Neill J J 1968 *RCA Rev.* **29** 566–81

- Waits R K 1978 *J. Vac. Sci. Technol.* **15** 179–87
- Wang W, Foster J, Snodgrass T, Wendt A E and Booske J H 1999 *J. Appl. Phys.* **85** 7556–61
- Wasa K and Hayakawa S 1967a *Proc. IEEE* **55** 2179–80
- Wasa K and Hayakawa S 1967b *Microelectron. Reliab.* **6** 213–21
- Wasa K and Hayakawa S 1969 *Rev. Sci. Instrum.* **40** 693–7
- Wendt A E 1988 Dynamics of a planar magnetron discharge *PhD Thesis* University of California at Berkeley, Berkeley, California
- Wendt A E, Lieberman M A and Meuth H 1988 *J. Vac. Sci. Technol. A* **6** 1827–31
- Westwood W D 1976 *Prog. Surf. Sci.* **7** 71–111
- Willmott P R and Huber J R 2000 *Rev. Mod. Phys.* **72** 315–28
- Window B and Savvides N 1986 *J. Vac. Sci. Technol. A* **4** 196–202
- Wright A W 1877 *Am. J. Sci.* **s3-14** 169–78
- Wright M and Beardow T 1986 *J. Vac. Sci. Technol. A* **4** 388–92
- Wu L, Ko E, Dulkan A, Park K J, Fields S, Leeser K, Meng L and Ruzic D N 2010 *Rev. Sci. Instrum.* **81** 123502
- Xu J, Deng X, Zhang J, Lu W and Ma T 2001 *Thin Solid Films* **390** 107–12
- Yamamura Y 1981 *Radiat. Eff. Defects Solids* **55** 49–55
- Yamamura Y, Takiguchi T and Ishida M 1991 *Radiat. Eff. Defects Solids* **118** 237–61
- Yamamura Y and Tawara H 1996 *At. Data Nucl. Data Tables* **62** 149–253
- Yang Y, Tanaka K, Liu J and Anders A 2015 *Appl. Phys. Lett.* **106** 124102
- Ye B *et al* 2021 *Rev. Sci. Instrum.* **92** 113906
- Yoshida Y 1992 *Appl. Phys. Lett.* **61** 1733–4
- Zhirkov I, Petruhins A and Rosen J 2015 *Surf. Coat. Technol.* **281** 20–6
- Ziegler J F, Biersack J P and Ziegler M D 2008 *SRIM—The Stopping and Range of Ions in Matter* (Chester, Maryland: SRIM Co.)
- Ziegler J F, Ziegler M D and Biersack J P 2010 *Nucl. Instrum. Methods Phys. Res. B* **268** 1818–23